ISTANBUL TECHNICAL UNIVERSITY ★ GRADUATE SCHOOL OF SCIENCE ENGINEERING AND TECHNOLOGY

VISION BASED POSITIONING ABB IRB 140 ROBOT FOR GAS LEAKAGE TEST AUTOMATION

M.Sc. THESIS

Akın İlker SAVRAN

Department of Control and Automation Engineering

Control and Automation Engineering Programme

JUNE 2018

ISTANBUL TECHNICAL UNIVERSITY ★ GRADUATE SCHOOL OF SCIENCE ENGINEERING AND TECHNOLOGY

VISION BASED POSITIONING ABB IRB 140 ROBOT FOR GAS LEAKAGE TEST AUTOMATION

M.Sc. THESIS

Akın İlker SAVRAN
(504151102)

Department of Control and Automation Engineering

Control and Automation Engineering Programme

Thesis Advisor: Assoc. Prof. Dr. Tufan KUMBASAR

JUNE 2018

İSTANBUL TEKNİK ÜNİVERSİTESİ ★ FEN BİLİMLERİ ENSTİTÜSÜ

GAZ KAÇAK TEST OTOMASYONU İÇİN ABB IRB 140 ROBOT İÇİN GÖRÜNTÜ TABANLI POZİSYONLAMA

YÜKSEK LİSANS TEZİ

Akın İlker SAVRAN
(504151102)

Kontrol ve Otomasyon Mühendisliği Anabilim Dalı

Kontrol ve Otomasyon Mühendisliği Programı

Tez Danışmanı: Doç. Dr. Tufan KUMBASAR

HAZİRAN 2018

Akın İlker Savran, a **M.Sc.** Student of ITU **Graduate School of Science Engineering and Technology** student ID **504151102**, successfully defended the **thesis/dissertation** entitled **"VISION BASED POSITIONING ABB IRB 140 ROBOT FOR GAS LEAK TEST AUTOMATION",** which he/she prepared after fulfilling the requirements specified in the associated legislations, before the jury whose signatures are below.

Thesis Advisor : **Assoc. Prof. Dr. Tufan KUMBASAR**
Istanbul Technical University

Jury Members : **Asst. Prof. Dr. Volkan SEZER**
Istanbul Technical University

Asst. Prof. Dr. Levent UCUN
Yildiz Technical University

Date of Submission : 4 May 2018
Date of Defense : 6 Jun 2018

To my family,

FOREWORD

I would like to thank all the people and institutions that have provided me with their support and assistance in this thesis process. I would like to show my gratitude to my thesis advisor Asst. Prof. Dr. Tufan Kumbasar for his encouragements, sincerity and guidance during the period of my university education. I would like to thank researcher Aykut Beke and labarator staff for their help, suggestions and support during my research work. Finally, I would like to thank my parents and my friends for their assistance and confidence.

I would like to thank Arçelik Dryer Factory provided to me in the scope of this project. I would like to thank Erdem Çelik and Ali Rıza Yilmaz, my managers who supported me during my thesis work. I would like to thank my friends of the automation team in Arçelik Özgür Erbulan, Ahmet Mücahit Polat and Ahmet Metin for their support in my thesis work.

May 2018 Akın İlker Savran

TABLE OF CONTENTS

Page

FOREWORD ..... **ix**
TABLE OF CONTENTS ..... **xi**
ABBREVIATIONS ..... **xiii**
SYMBOLS ..... **xv**
LIST OF TABLES ..... **xvii**
LIST OF FIGURES ..... **xix**
SUMMARY ..... **xxi**
ÖZET ..... **xxv**
1. INTRODUCTION **1**
2. ABB IRB 140 INDUSTRIAL ROBOT **7**
2.1 Hardware 7
2.2 Coordinate Systems 10
2.2.1 Tool center point 10
2.2.2 Base coordinate system 11
2.2.3 World coordinate system 11
2.2.4 Work object coordinate system 12
2.2.5 Tool coordinate system 13
2.3 Modeling 13
2.3.1 Kinematic modeling 13
2.3.2 Dynamic modeling 16
2.4 Programming and PLC implementation 18
3. IMAGE PROCESSING METHOD AND CAMERA CALIBRATION **21**
3.1 Threshold 21
3.2 Morphological Operator 22
3.2.1 Dilation operator 23
3.2.2 Erosion operator 23
3.2.3 Opening operator 24
3.2.4 Closing operator 25
3.3 Color Plane Extraction 26
3.4 Camera Calibraition 27
3.4.1 Basic camera model 27
3.4.2 Pinhole camera model 28
3.4.3 Coordinate transformation 29
3.4.4 Application of camera calibration 30
4. GAS LEAKAGE TEST STATION **33**
4.1 Heat Pump Dryer 33
4.2 Gas Leakage Test 34
4.3 Vision Based Positioning 36
4.4 Image Processing Algorithm for Welding Points of Gas Leakage Test 39
4.4.1 Image processing algorithm for first area 40

4.4.2 Image processing algorithm for second area 43
4.4.3 Image processing algorithm for third area 45
5. EXPERIMENTAL RESULTS 49
5.1 Updating The Camera Calibration Parameters 49
5.2 High Pressure Test Results 50
5.3 Equilibrium Test Results 56
6. CONCLUSION 63
REFERENCES 67
CURRICULUM VITAE 71

ABBREVIATIONS

CNC **:** Computer Numerical Control
DOF : Degree of Freedom
TCP **:** Tool Center Point
DH **:** Denavit Hartenberg
GUI **:** Graphical User Interface
VC **:** Virtual Controller
IRC **:** Industrial Robot Controller
PLC **:** Programming Logic Controller
RGB **:** Red Green Blue
HP **:** Heat Pump
NI **:** National Instruments
HSL **:** Hue Saturation Luminence
LUT **:** LookUp Table

SYMBOLS

P_{xw}, P_{yw}, P_{zw}	: The position of wrist center
g	: Smooth matrix function
h	: Smooth function
A	: Image set
B	: Structuring element
α	: The distance between lens and object
β	: The distance between lens and image
f	: Focal length
λ	: Wavelength of incoming light
D	: Diameter of gap
P (X, Y, Z)	: World coordinate system
P_c, **(X, Y, Z)**	: Camera coordinate system
P (u, v)	: Pixel coordinate system
R	: Rotaional matrix
T	: Translational matrix
C_x, C_Y	: Coordinate value corresponding ro origin in the image

LIST OF TABLES

Page

Table 2.1 : DH parameter of IRB140 robot 14
Table 4.1 : Classification of source points according to test type. 35
Table 5.1 : Camera calibration parameters. 50
Table 5.2 : The descriptive statictics of deviations on the X axis for high pressure. 55
Table 5.3 : The descriptive statictics of deviations on the Y axis for high pressure. 56
Table 5.4 : The descriptive statictics of deviations on the X axis for equilibrium. .. 61
Table 5.5 : The descriptive statictics of deviations on the Y axis for equilibrium. .. 61

LIST OF FIGURES

Page

Figure 2.1 : The controller of ABB IRB 140 Robot. 8
Figure 2.2 : The ABB IRB 140 Robot. 9
Figure 2.3 : The gripper of ABB IRB 140 Robot. 9
Figure 2.4 : The illustraion of tool center point. 10
Figure 2.5 : The illustration of base coordinate system. 11
Figure 2.6 : The illustration of world coordinate system. 12
Figure 2.7 : The illustarion of work object coordinate system. 12
Figure 2.8 : The illustration of tool coordinate system. 13
Figure 2.9 : Kinematic structure and frame assigments of the ABB IRB140 robot. 14
Figure 2.10 : Projection of the wrist center onto the xy plane. 15
Figure 2.11 : The overview of robot control. 18
Figure 2.12 : Communication network of test station. 19
Figure 2.13 : PLC program structure of test station. 20
Figure 3.1 : The effect of dilation operator. 23
Figure 3.2 : The effect of erosion operator. 24
Figure 3.3 : The effect of opening operator. 25
Figure 3.4 : The effect of closing operator. 26
Figure 3.5 : The illustration of lens law. 27
Figure 3.6 : The coordinate systems of pinhole camera model. 28
Figure 3.7 : The grid partition on the world coordinate system 31
Figure 4.1 : The heat pump dryer. 33
Figure 4.2 : The chassis of heat pump dryer. 34
Figure 4.3 : The welding points of gas leakage test. 35
Figure 4.4 : The gas leakage test station. 37
Figure 4.5 : The flowchart of test station 38
Figure 4.6 : The divided areas for image processing algorithms. 39
Figure 4.7: The labview block diagram. 40
Figure 4.8 : The image mask and color plane extraction operators for first area. 41
Figure 4.9 : The grayscale morphological and threshold operators for first area. 41
Figure 4.10 : The first dilate and remove small objects operators for first area. 42
Figure 4.11 : The second dilate and remove small objects operators for first area. . 42
Figure 4.12 : The LUT and max clamp operator for first area. 43
Figure 4.13 : The image mask and color plane extraction operators for second are 43
Figure 4.14 : The grayscale morphological and threshold operators for second are 44
Figure 4.15 : The close and remove small objects operators for second area. 44
Figure 4.16 : The dilate and particle filter operators for second area. 45
Figure 4.17 : The LUT and max clamp operators for second area 45
Figure 4.18 : The image mask and color plane extraction operators for third area. . 46
Figure 4.19 : The grayscale morphological and threshold operators for third area. . 46
Figure 4.20 : The close and remove small objects operators for second area. 46

Figure 4.21 : The dilate and erode operators for third area. 47
Figure 4.22 : The LUT and max clamp operators for second area. 48
Figure 5.1 : The deviation (a) all (b) peak first welding points on X axis. 50
Figure 5.2 : The deviation (a) all (b) peak first welding points on Y axis. 51
Figure 5.3 : The deviation (a) all (b) peak second welding points on X axis. 52
Figure 5.4 : The deviation (a) all (b) peak second welding points on Y axis. 52
Figure 5.5 : The deviation (a) all (b) peak sixth welding points on X axis. 53
Figure 5.6 : The deviation (a) all (b) peak sixth welding points on Y axis. 53
Figure 5.7 : The deviation (a) all (b) peak seventh welding points on X axis. 54
Figure 5.8 : The deviation (a) all (b) peak seventh welding points on Y axis. 55
Figure 5.9 : The deviation (a) all (b) peak third welding points on X axis. 57
Figure 5.10 : The deviation (a) all (b) peak third welding points on Y axis. 58
Figure 5.11 : The deviation (a) all (b) peak fourth welding points on X axis. 59
Figure 5.12 : The deviation (a) all (b) peak fourth welding points on Y axis. 59
Figure 5.13 : The deviation (a) all (b) peak fifth welding points on X axis. 60
Figure 5.14 : The deviation (a) all (b) peak fifth welding points on Y axis. 60

VISION BASED POSITIONING ABB IRB 140 ROBOT FOR GAS LEAKAGE TEST AUTOMATION

SUMMARY

Technological progress has been recorded in factories over the past decade. Dangerous, repetitive and difficult tasks on production lines are carried out by automatic machines instead of people. The industrial robots provide significant flexibility and adaptability in production lines. With robotic working conditions, increased productivity and quality, independent production from the human labor force will take place. There will be integrated factories that are compatible with the Factory of Futures. The factories will use robots in a variety of tasks, and many research and development, performance improvement and complex control algorithms for robots are still being developed. It begins with the use of industrial robots in General Motors in 1961 for use in production lines. The first patent of industrial robots was taken by George Devol in 1965. Today, the number of industrial robots is increasing, especially in the automotive sector. By the end of 2017, a total of nearly 2 million industrial robot are being used.

One of the benefits provided by the using robots is that movements are reproducible, accurate and reliable. However, it has been seen that robots do not work successfully in situations that change if they work on their own. According to the changing conditions, manual teaching will not be a solution because it takes a long-time procedure and processes that affect it completely. For this reason, it is one of the most important issues to be notified about the environment of robots in the automation processes, examples of which are vision based positioning robots.

Computer vision applications contains methods for processing, analyzing and understanding images. High-dimensional data from the real world is often used to generate numerical and symbolic information with decision forms. The increasing use of these applications is a perception of the underlying vision of a computer vision. Computer vision applications are used in industry, medicine and robot technology. Vision based robot positioning started to be used in the early 1970s. Many working systems and approaches have been proposed theoretically and technically in image processing such as positioning and depth adjustment, feature selection and processing, camera models and calibration.

In this thesis, firstly, a 6-axis ABB IRB 140 robot which are 3 are translational and 3 are rotational for robotic automatic test system is presented. ABB IRB 140 robot consists of 5 main parts. The first one is the controller of the robot where the robot is programmed and the drivers are found. The second one is robot arms where robot movements are made. The robot determines the mobility, its accessibility, and the maximum capacity according to the size and shape of the robot arms. The third is the drivers that determine the speed and acceleration of robot movements. The fourth is the gripper which is added to the tip of the robot and changes its relative position. A gas leak detector was used in this study. Finally, the sensors measure the speed and

acceleration of the robot. Robot movements and target positions are defined in coordinate systems. Robots allow to work in many coordinates. These are base, world, work object and tool coordinate systems. The target position of the robots is determined according to the final position of the vehicle attached to the robot end effector, and this point is called the tool center point. The world coordinate system is used as the coordinate system in ABB IRB 140 robot. The kinematic and dynamic models of ABB IRB 140 are given. In the kinematic model of the robot there is a simplification of the mathematical Denavit Hartenberg algorithm. In this model, the robot calculates the position of the robot center point in the coordinate system depending on the joints. In the dynamic model, the interaction of the joints expressing the interaction of the joints is given. The ABB IRB 140 robot is programmed using the RAPID programming language. Robot relates to TCP-IP connection protocol and programmed in RoboStudio program on robot computer and the program of robot is installed. The ABB IRB 140 robot works in this project with an automation system in which the PLC and camera are controlled PC module. For this reason, the robot has been implemented with PLC. Robot receives all signals and information from PLC via Profinet communication protocol.

In the second stage of the thesis study, image processing algorithms are explained and coordinate transformation and camera calibration are done. Digital image processing algorithms have been used in this study. These methods are threshold, morphological operators and color plane extraction methods. In the threshold method, segmentation is performed by assigning two or more classes of each pixel in the source image to the color images from the grayscale image. This method divides the image intended for processing by using at least one color or gray scale value. Morphological operators are an effective image processing method in nonlinear neighborhood processing. In morphological operators which are dilation, erosion, opening and closing operators are used. The size of the objects is enlarged in the dilation operator, and the size of the objects is reduced in the erosion operator. In the opening operator, objects close to each other are removed without any change, while objects in close operators are connected to each other. With the color plane extraction method, the color information is obtained. The positions obtained in the image processing method are included in the image coordinate system. However, the positions in the ABB IRB 140 program are defined in the world coordinate system. For this reason, coordinate transformation is performed with linear equations. Subsequently, the camera calibration for the coordinate transformation was done on a grid plane and the parameters were found. These parameters have been updated according to the depth change in the algorithm.

At the next stage of the thesis work, a gas leakage test is carried out using robotic automation. In the heat pump dryer, the air in the drum has air flow to raise the air temperature and to extract the air from the ambient air, with the heat pump compressor. The heat pump dryer consists of compressor, condenser, evaporator and copper pipes connecting them. There are welding points on the copper pipe where the components are connected to each other. In this study, these welding points will be leak tested with ABB IRB 140 robot. Two types of tests are presented, which are the high pressure test and the equilibrium test. Firstly, a high pressure test will be performed. In this test, four welding points on the copper pipe leading to the condenser from the compressor are tested. The test is done when the gas in the pipe is between 15-20 bars behind the compressor stop. Secondly, the equilibrium test is performed. This test is performed by testing the 3 welding points of the pipe coming

out from the compressor to evaporator. The test is made 10 seconds after the compressor stops and the high pressure test. The gas pressure in the pipe goes up to 9 bar. The positions of the welding points are varied due to various reasons. In this thesis, ABB IRB 140 robot system with vision based positioning is presented to provide the flexibility of correcting the gas leakage tests with robotic automation. The vision based positioning is to obtain position information from the image processing algorithm of the target robot. In this study, a single camera was used and the camera is mounted in a fixed position.

In addition, in this thesis, the area of the welding points is divided into 3 according to the depths of the points and image processing algorithms are formed for each area. Algorithms re done with the NI Vision Assistant application and run in sequence in the Labview program. In the three image processing algorithms, mask operations are used in the original image to initially constrain the restrictive rectangle. The threshold operator is used to make the copper pipe visible. The threshold operator parameters are 72, 82 and 93, respectively. After the threshold method, the morphological operators are applied more than once in the same algorithm to protect the welded pipes and to sift the images with threshold values close to the copper pipe. After the copper pipe was obtained, the Lookup table was applied to the image obtained to change the dynamic intensity of the field in the image. After applying the lookup table, the original image is overlaid with the image obtained in the algorithm after the color plane of the image is extracted. Finally, it has been applied to three image processing algorithms to determine the welding points in the field with the maximum clamping operator.

Finally, for demonstrating the performance of the gas leakage test with ABB IRB 140 robot with the vision based positioning, real-time experiment work has been carried out. The real-time experiments were performed by collecting the position data of 500 welding points and graphically and statistically examining the position data. The experimental results showed that the ABB IRB 140 robot application with image-based positioning was successful in capturing position deviations and performing the test. In the experiments, parameter update was done firstly according to the depth value in image processing areas. Secondly, the deviations of the welding points in the high pressure test have been investigated. In this test, it is seen that the deflection amount at the 6. and 7. welding points is more in the X axis. Then, the amount of deviations of the 1. and 2. welding points is less in the X axis. In the high pressure test, there is a minimum deviation of -187.8 mm and a maximum of 165.5 mm on the X axis. For this reason, it was observed that the ABB IRB 140 robot with vision based positioning on the X axis is successful. In the high-pressure test, the deviations of the 4 welding points are observed on the Y-axis but less than the X axis. At the welding points, a minimum deviation of -76.49 mm and a maximum of 92.43 mm was observed on the Y-axis. Third, the position deviation values of the welding points in the equilibrium test are examined. In this test, the amount of deviations of the 5. welding point is found to be larger that 3. and 4. welding points on the X axis. the amount of deviations on the X axis was observed to be less for at the 3. and 4. welding points. There is a minimum deviation of -122.8 mm and a maximum of 93.26 mm on the X axis. For this reason, it was observed that the ABB IRB 140 robot with image-based positioning on the X-axis was successful. At these welding points, the minimum deviation is -76.76 mm and the maximum deviations 77.03 mm was observed on the Y-axis.

In summary, ABB IRB 140 robot application with vision based positioning for gas leak test has been realized in this Master thesis. In this study, a 6-axis ABB IRB 140 robot is used, the image processing algorithms are created to find the welding points on the copper pipe, the coordinate transformation is made between the camera and the robot, and position deviations are examined in real time applications to demonstrate the success of the application.

GAZ KAÇAK TEST OTOMASYONU İÇİN ABB IRB 140 ROBOT İÇİN GÖRÜNTÜ TABANLI POZİSYONLAMA

ÖZET

Son on yıl içerisinde fabrikalarda teknolojik anlamda ilerlemeler kaydedilmiştir. Üretim hatlarında tehlikeli, tekrarlayan ve zor görevler insanlar yerine otomatik makineler tarafından gerçekleştirilmektedir. Endüstriyel robotlar üretim hatlarında ciddi esneklik ve uyarnabilirlik sağlamaktadır. Robotların çalışma koşulları, verimliliğin ve kalitesinin artması ile beraber insan iş gücünden bağımsız üretimler gerçekleşecektir. Geleceğin fabrikası konseptine uygun birbirine entegre fabrikalar oluşacaktır. Fabrikalarda çeşitli görevlerde robotlar kullanılacaktır ve günümüzde robotlar için birçok araştırma ve geliştirme, performans iyileştirme ve kompleks kontrol algoritmalarının geliştirilmesi devam etmektedir. Endüstriyel robotların üretim hatlarında kullanılmasına 1961 yılında General Motor'da kullanılması ile başlamaktadır. Endüstriyel robotların ilk patenti ise 1965 yılında George Devol tarafından alınmıştır. Başlangıçta robotlar otomotiv sektörde spot kaynak işlemlerinde kullanılmışlardır. Bilgisayar ile kontrol edilen robotlar 1973'de mikrobilgisayar tabanlı kontrol ile IRB-6 endüstriyel robotlar olarak yapılmıştır. Günümüzde endüstriyel robotların sayıları başta otomotiv sektörü olmak üzere giderek artmaktadır. 2017 yıl sonunda toplam 2 milyona yakın endüstriyel robot üretim hatlarında kullanılmaktadır.

Robotların kullanılması ile sağlanan faydalardan biri hareketlerin tekrarlanabilirliği, doğru ve güvenilebilir olarak gerçekleşmesidir. Ancak robotların kendi başına çalışması durumunda değişiklik gösteren durumlarda başarılı çalışmadığı görülmüştür. Değişen koşullara göre manuel öğretme çok zaman alan prosedür ve etkileyen süreçlerin tamamen önlenmesi gerektiği için çözüm olmayacaktır. Bu nedenle otomasyon süreçlerinde robotların çevrelerinden haber edilmesi en önemli konulardan biridir, bu uygulamalardan örnek olarak görüntü tabanlı pozisyonlanmalı robotlar örnek verilebilir.

Bilgisayar tabanlı görüntü uygulamaları görüntü işlemek, analiz etmek ve anlamak için yöntemler içeren uygulamalardır. Gerçek dünyadan gelen yüksek boyutlu verilerin genellikle karar formları ile sayısal ve sembolik bilgi üretmek için kullanılır. Bu uygulamaların kullanımının artmasının nedeni bir görüntünün bilgisayar vizyonu ile algılanma becerisidir. Bilgisayar görüntü tabanlı uygulamalar endüstri, tıp ve robot teknolohisinde kullanılmaktadır. Görüntü tabanlı robot pozisyonlama 1970'lerin başlarında kullanılmaya başlanmıştır. Pozisyonlama ve derinlik ayarlanması, özellik seçimi ve işleme, kamera modelleri ve kalibrasyon gibi görüntü işleme alanında teorik ve teknik yönlenerden birçok çalışma sistemi ve yaklaşım önerilmiştir. Görüntü tabanlı robotik uygulamalarda ilerlemeler olmasına rağmen az sayıda endüstriyel uygulama yapılmıştır. Çalışmaların çoğu araştırma amaçlı olmuştur ve labarotuar ortamlarında denenmiştir. Görüntü tabanlı robotik

endüstriyel uygulamalardan örnek olarak konveyöre ürün koyma, parça çiftlemesi ve otomatik testler verilebilir.

Bu tez çalışmasında ilk olarak, robotlu otomatik test sistemi için kullanılan 6 eksenli ABB IRB 140 robot sunulmuştur. Robotun 6 ekseninden 3 tanesi translasyon hareket, 3 tanesi ise rotasyon hareketi sağlamaktadır. ABB IRB 140 robot 5 ana bölümden oluşmaktadır. Birincisi robotun programlandığı ve sürücelerin bulunduğu robotun kontrolcüsüdür. İkincisi robot hareketlerinin yapıldığı robot kollarıdır. Robotun hareket kabileyetini, erişebilirliğini ve taşıyacağı maksimum kapasiteyi robot kollarının boyutu ve şekili belirler. Üçüncüsü robot hareketlerinin hızını ve ivmesini belirleyen sürücülerdir. Dördüncü ise robotun ucuna eklenen ve göreve değişiklik gösteren gripperdır. Bu çalışmada gaz kaçak dedektörü kullanılmıştır. Son olarak robotun hızını ve ivmesini ölçen sensörlerdir. Robotların hareketleri ve hedef pozisyonları koordinat sistemlerinde tanımlanmaktadır. Robotlar pek çok koordinat alınanda çalışmasına olanak sağlar. Bunlar base, dünya, çalışma objesi ve araç koordinat sistemleridir. Robotların hedef konumu robot ucuna eklenen aracın son pozisyonuna göre belirlenmektedir ve bu noktaya araç merkez noktası denmektedir. ABB IRB 140 robotta koordinat sistemi olarak dünya koordinat sistemi kullanılmıştır. ABB IRB 140 robotunun kinamatik ve dinamik modelleri verilmiştir. Robotun kinematik modelinde matematiksel Denavit Hartenberg algoritmasının sadeleştirilmiş hali mevcuttur. Bu modelde giriş eklem açılarına bağlı olarak robot araç merkez noktasının koordinat sisteminde ulaşacağı pozisyonu hesaplamaktadır. Dinamik modelde ise eklemlerin birbiri ile etkileşimini ifade eden bağlantılı eklemlerin etkileşimi verilmektedir. ABB IRB 140 robot RAPID programlama dili kullanılarak programlanmıştır. Robota TCP-IP bağlantı protokolü ile bağlanılarak robot bilgisayar üzerinde RoboStudio programında programlanmış ve program robota yüklenmiştir. ABB IRB 140 robot bu projede bir otomasyon sisteminde PLC ve PC modülü kontrol edilen kamera ile birlikte çalışmıştır. Bu nedenle robotun PLC ile implementasyonu yapılmıştır. Robot bütün sinyalleri ve bilgileri PLC'den Profinet haberleşme protokolü ile almaktadır. Robota kameradan pozisyon bilgileri, PLC'den ise robotun teste başlama sinyali gelmektedir. Robottan ise PLC'ye testin tamamlandı sinyali gelmektedir.

Tez çalışmasının ikinci aşamasında ise görüntü işleme algoritmları anlatılmış ve koordinat transformasyonu ve kamera kalibrasyonu yapılmıştır. Bu çalışmada dijital görüntü işleme algoritma yöntemleri kullanılmıştır. Bu yöntemler ise eşik, morfolojik işlemler ve renk düzlemi çıkarma yöntemleridir. Eşik yönteminde gri tonlamalı görüntüden kaynak görüntüdeki her pikselin iki veya daha fazla sınıfını renkli görüntülerde atama işlemi olan segrementasyon yapılır. Bu yöntem görüntü işlemede amaçlanan görüntünün sınırlayarak en az bir renk veya gri skala değeri kullanarak bölmektir. Morfolojik işlemler lineer olmayan komşuluk işlemlerinde etkili bir görüntü işleme yöntemidir. Morfolojik işlemlerde genişletme, aşındırma, açma ve kapama işlemleri kullanılmaktadır. Genişletme işleminde objelerin boyutu büyütülmektedir, aşındırma işleminde ise objelerin boyutu daraltılmaktadır. Açma işleminde birbirine yakın nesneler değişim uygulanmadan ayrılır, kapa işleminde ise birbirine yakın nesneler bağlanmaktadır. Renk düzlemi çıkarma yöntemi ile görüntükdeki renk bilgisi elde edilmektedir. Görüntü işleme yönteminde elde edilen pozisyonlar resim koordinat sisteminde yer almaktadır. Ancak ABB IRB 140 programında pozisyonlar dünya koordinat sisteminde tanımlanmaktadır. Bu nedenle lineer denklemler ile koordinat dönüşümü yapılmıştır. Sonrasında koordinat dönüşümü için kamera kalibrasyonu grid parçalı düzlemde yapılmıştır ve

parametreler bulunmuştur. Bu parametreler algoritmada derinlik değişimine bağlı olarak güncellenmiştir.

Tez çalışmasının sonraki aşamasında robotlu otomasyon uygulanmasının yapıldığı gaz kaçak testi sunulmuştur. Isı pompalı kurutma makinasında tambur içerisindeki hava sıcaklığı yükseltmek ve ortam havasında hava çıkarmak ısı pompası buharlaştırıcınsa sahip hava akışına sahiptir. Isı pompalı kurutma makinası şasisi kompresör, kondanser, evaoperatör ve bunları birbirine bağlayan bakır borulardan oluşmaktadır. Bakır boru üzerinde komponentlerin birbirine bağlandığı noktalarda kaynak noktaları bulunmaktadır. Bu çalışmada bu kaynak noktaları ABB IRB 140 robot ile sızdırmazlık testi yapılacaktır. İki tip test sunulmuştur, bu testler yükse basınç testi ve denge testidir. İlk olarak yüksek basınç testi yapılacaktır. Bu teste kompresörden çıkan kondansere giden bakır boru üstünde bulunan 4 kaynak noktası test edilmektedir. Test kompresörün durmasının ardında borudaki gazın 15-20 bar arasındayken yapılır. İkinci olarak denge testi yapılır. Bu teste kompresörden çıkan evaoperatöre çıkan borudaki 3 kaynak noktasının testi yapılmaktadır. Test kompresörün durmasından 10 saniye sonra ve yüksek basınç testinden sonra borudaki gaz basıncının 9 bar seviyesine çıkması ile yapılmaktadır. Kaynak noktaların pozisyonlarında çeşitli sebeplerden dolayı değişiklik bulunmaktadır. Gaz sızdırmazlık testlerinin robotlu otomasyon ile yapılmasından doğruluğu esnekliği sağlamak için bu tezde görüntü tabanlı pozisyonlamalı ABB IRB 140 robot sistemi sunulmuştur. Görüntü tabanlı pozisyonlamalı yönteminin amacı robotun görüntü işleme algoritmasından konum bilgilerinin elde edilmesidir. Bu çalışmada tek kamera kullanılmıştır ve kamera sabit bir pozisyonda sabitlenmiştir.

Ayrıca bu tezde kaynak noktalarının bulunduğu alan noktaların derinliklerine göre 3'e ayrılmıştır ve her bir bölge için görüntü işleme algoritmaları oluşturulmuştur. Algoritmalar NI Vision Assistant uygulaması ile yapılmıştır ve Labview programında sırasıyla çalıştırılmıştır. Üç görüntü işleme algoritmasında, ilk olarak, kısıtlayıcı dikdörtgeni sınırlamak için orijinal görüntüde maske işlemleri kullanılır. Eşik operatörü, görüntüdeki bakır borunun görünür hale getirilmesi için kullanılır. Eşik operatörü parametreleri 72,82 ve 93 olarak seçilmiştir. Eşik yönteminden sonra, morfolojik operatörler, bakır boruya yakın eşik değerine sahip görüntüleri elemek ve kaynak yapan boruları korumak için aynı algoritmada birden fazla kez uygulanmıştır. Bakır boru elde edildikten sonra, arama tablosunda görüntüde alanın dinamik yoğunluğunu değiştirmek için elde edilen görüntüye uygulandı. Arama tablosunun uygulanmasından sonra görüntüyü renk düzlemi çıkarıldıktan sonra algoritmalarda elde edilen görüntü ile orijinal görüntü üst üste bindirilmektedir. Son olarak, maksimum kenet operatörü ile alan içerisindeki kaynak noktalarını belirlemek için üç görüntü işleme algoritmasında da uygulanmıştır.

Son olarak, görüntü tabanlı pozisyonlanmalı ABB IRB 140 robot ile yapılan gaz sızdırmazlık testinin başarımlarını göstermek amacıyla, gerçek zamanlı deney çalışmaları gerçekleştirilmiştir. Gerçek zamanlı deneyler 500 adet üründen kaynak noktalarının pozisyon verileri toplanarak ve pozisyon verilerinin grafiksel ve istatiksel olarak incelenmiştir. Deney sonuçları göstermiştir ki görüntü tabanlı pozisyonlanmalı ABB IRB 140 robot uygulaması pozisyon sapmalarını yakalaması ve testin gerçekleşmesi bakımından başarılı olmuştur. Deney çalışmalarında ilk olarak görüntü işleme alanlarındaki derinlik değerine göre parametre güncellemesi yapılmıştır. İkinci olarak yüksek basınç testinde bulunan kaynak noktalarındaki sapmalar incelenmiştir. Bu testte özellikle 6. ve 7. kaynak noktalarında sapma miktarı X ekseninde fazla olduğu görülmüştür. Bu nedenin olarak kondenselerde

farklı tiplerde kondenserlerin kullanılmasıdır. 1. ve 2. kaynak noktlarında ise X ekseninde sapma miktarı daha az olduğu gözlemlenmiştir. Bu kaynak noktalarında ürün içerisinde palet üzerinde şasi hareketleri ve paletlerdeki boyut farklıklıkları olduğu belirtelebilir. Yüksek basınç testinde X ekseninde minimum -187.8 mm ve maksimum 165.5 mm sapma olmaktadır. Bu sebeple X ekseninde görüntü tabanlı poziyonlamalı ABB IRB 140 robot çalışmasının başarılı olduğu gözlemlenmiştir. Yüksek basınç testinde Y ekseninde ise 4 kaynak noktasında da sapmaların sebebi olarak şasi içinde kompresör ve kondanserin hareketliği ve palet boyut farklılıkları belirtilmiştir. Kaynak noktalarında Y ekseninde minimum -76.49 mm ve maksimum 92.43 mm sapma gözlenmiştir. Üçüncü olarak denge testindeki kaynak noktalarının pozisyon sapma değerleri incelenmiştir. Bu testte 5. kaynak noktasında sapma miktarı X ekseninde fazla olduğu görülmüştür. Bu nedenin olarak evaoperatörde farklı tiplerde evaoperatörün kullanılmasıdır. 3. ve 4. kaynak noktlarında ise X ekseninde sapma miktarı daha az olduğu gözlemlenmiştir. Bu kaynak noktalarında ürün içerisinde palet üzerinde şasi hareketleri ve paletlerdeki boyut farklıklıkları olduğu belirtelebilir. Denge testinde X ekseninde minimum -122.8 mm ve maksimum 93.26 mm sapma olmaktadır. Bu sebeple X ekseninde görüntü tabanlı poziyonlamalı ABB IRB 140 robot çalışmasının başarılı olduğu gözlemlenmiştir. Yüksek basınç testinde Y ekseninde ise 3 kaynak noktasında da sapmaların sebebi olarak şasi içinde kompresör ve kondanserin hareketliği ve palet boyut farklılıkları belirtilmiştir. Kaynak noktalarında Y ekseninde minimum -76.76 mm ve maksimum 77.03 mm sapma gözlenmiştir.

Bu çalışmada özetle, gaz kaçak testi için görüntü tabanlı pozisyonlanmalı ABB IRB 140 robot uygulaması gerçekleşmiştir. Bu çalışma içerisinde 6 eksenli ABB IRB 140 robot kullanılmış, bakır boru üzerindeki kaynak noktalarının bulunması için görüntü işleme algoritması oluşturulmuş, kamera ile robot arasında koordinat dönüşümü yapılmış ve uygulanmanın başarısının gösterilmesi için gerçek zamanlı uygulamalarda pozisyon sapmaları incelenmiştir.

1. INTRODUCTION

Today's production facilities have been leaping in a major automation trend in a few decades. The role of people on dangerous, repetitive or tiring assignments has been given to automatic machines. The industrial robots have much more adaptability and flexibility with respect to all the machines in production and assembly lines. It must become increasingly independent from human intervention to improve working conditions, productivity and quality of the machine and robots, and create an integrated and interdependent entity that will gradually become the Factories of Future [1]. It is envisaged that robots will be used in various jobs in a plurality of factories. Nowadays, many research and development are going to improve their designs, control algorithms and performance. One of the most important things in automated production is that more awareness of robots than their environments. Being in communication with the tools that the robots work with is one of the most important methods for ensuring this [2].

Nowadays, industrial robots have the capacity to carry out many tasks. This is one of the important advantages in using robots. Often, a robot is used to perform various assignments on different objects or different stages of the workflow. In the automated process, tool changer systems are used for a variety of tools of robots using. The accuracy of reproducibility which is quality criteria in these flexible automated industrial production lines [3]. The robot determines the limits to achieve accurate and reliable movements in the process that accuracy of reproducibility of robot can be used. Manual teaching procedures or offline programming are used the creation of robot programming.

The purpose of robot investments is usually to ensure earnings during working time. It can work for a long time without need for breaks the robot compared to the working order of a person. Production faults caused by human errors are reduced by the correct execution of the tasks of the robots. As a generally rule, it is estimated that the value produced in the automobile production line is 50,000 pairs per minute. This applies to producing a standard for primed automobiles [4]. The reason for this

is stated that a standard car in general has a shorter run time than a premium automobile. Thus, the loss due to production down time that cannot bring back for this reason, costs resulting from stoppages can cause serious effects in a short time. For this reason, reducing production downtime is one of the biggest goals. The quality error is one of the factors that affect production in a similar way. If the product does not have the qualification for quality maintenance, the product should be separated [5].

With fast and simple methods, stopping in robotic systems can be prevented [6].

- If the robot fails, the robot can be replaced.
- The calibration of the robot program can be verified at scheduled intervals. This means that the quality of robot movements can be achieved with frequent calibrations.
- Quickly calibrating changes in the robot's program helps to reduce the cost due to downtime.
- The robot program can be modified such that the robot can be changed without having to re-adjust the programmed position.

Industrial robots were first implemented in the manufacturing process with the first industrial Robot in 1961 General Motors production process [7]. An industrial robot patent was first introduced by George Devol on a programmed article in 1954 on a programmed entropy and given in 1961 [8]. Devol, together with Joseph Engelberger, founded the Unimate company and produced the Unimate robots which are hydraulically operated and are mainly used for spot welding in the automotive industry [9]. The IRB-6 industrial robot controlled by a microcomputer and driven electrically was introduced in 1973. It did not only allow simple point-to-point movements, however it also allowed for more complicated movements for the seam welding [7]. robots are widely used on production lines industries in ever growing numbers. According to The World Robotics Report 2014, total number of 178,132 new industrial robots in the 2013, with a total of over 1.3 million devices in use worldwide [10]. The investments are increasingly being made to automate production in all industries, especially in the automotive industry is still the largest branch of robots [11].

Every robot producer has begun to develop their own programming language, often inspired by one of the popular general-purpose programming languages. Some of these robot programming languages are RAPID is used for ABB robots [12], KRL is used for KUKA robots [13], Karel is used for FANUC robots and VAL3 is used for Staubli robots [14]. All these programming languages have a common point; conforms to the requirements of robotic applications. All languages have singular instructions for movements, and it is often possible to mix one move into another by marking the move as collapsible. A specific execution semantic is applied because motion commands can no longer exclusively be carried out before other commands. The next motion is known and planned unavoidably before completing the current one to let for motion blending. Skipping unnecessary motion commands and backward execution of robot program are common a non-standard feature in the programming language is used, for example, to correct mispositioned positions in the test phase. The programming languages of all robot brands are different and incompatible. For this reason, it is difficult to use more than one brand robot at the same time. If you want to use a different brand robot, you will have to learn the programming language of the new robot even if you have experience in previously used robot programming languages [11].

Vision-based robot positioning contains matching a group of image features to robot motion commands. The mapping between these two continuous fields is not highly linear, and it is very difficult - if not impossible - to derive analytically, depending on the nature of the properties used. This is especially true if global image identifiers are used as properties. There may be clear analytical relationships between camera exposure and image coordinates for local geometric features such as dots and lines [15].

A computer vision is a field that contains methods for processing, analyzing and acquiring and understanding images. High-dimensional data from the real world is used generally to generate numerical or symbolic information such as decision forms. The purpose of development of this field has been to increase understanding an image and the skills of the human vision by electronically perceiving. The applications of computer vision techniques are carried out by industry, medical field, robotics technology and so on [16]. Computer Numerical Control (CNC) machine must work at a fast face with minimum error and accuracy is important in

manufacturing process in several industries. For this reason, the computer vision is the key role of machine tools that can work in intelligent systems, increase correctness and avoid errors that happen with machine tools to speed up. his system uses the image processing technique to analyze the images to determine the characteristics of the 2D images of the images which extracts the object's property. The 2D feature extraction module extracts the object's property. The properties of the image properties are processed to aid in object recognition and segmentation include points of interest, edges, and corners [17].

Vision-based robot positioning is quite extensive with some of the oldest works dating back to the early 1970s. Many working systems and approaches have been proposed for certain theoretical and technical directions in vision processing and control areas such as pose and depth estimation, feature selection and processing, stereo vision and camera models and calibration [18]. Although significant progress has been recorded in the field, very little real industrial application of vision-based robotic systems has been performed up to now. Most of them have been research-focused and have been tested only in simulated and simplified laboratory environments such as inverted pendulum balancing, juggling and ball catching. Some of industrial applications of vision based robot positioning are welding, conveyor-belt picking [19], automated inspection [20], part mating, sealant application and fruit harvesting [21].

In this thesis, the automation project with vision based positioning by using ABB IRB 140 robot, which is given kinematic and dynamical models, is presented for gas leakage test for heat pump dryers. The robot coordinate planes are described and the world coordinate system is used for ABB IRB 140 robot in this study. The ABB IRB 140 Robot is programmed by using the RAPID program and the communication of the robot with the camera and PLC is provided by using Profinet communication protocol. Then, the methods are applied in the image processing algorithm are explained. For the camera calibration, the grid portion surface is used and the transformation between the image coordinate plane and the world coordinate system of ABB IRB 140 is completed with the coordinate transformations. This transformation is updated from the distance in a certain Z direction to the distance in the Z direction of the welding points to be tested in practice. After that, the heat pump dryer is introduced. The chassis of the dryer consists of compressor, condenser

and evaporator and these components are connected to each other by copper pipes and welded at connection points. The gas leakage test at the welding points is made gas leak detector device added to the end effector of ABB IRB 140 robot. Two types of tests have been defined due to the pressure difference in the cooper pipes. These tests are high pressure test has four welding points and equilibrium test has three welding points. With the same detector, these tests are carried out in succession by ABB IRB 140 robot.

Moreover, there are position changes at the welding points because of the use of components in different sizes in different models, due to position deviations on the pallet of the product and size differences in the pallets. The vision based positioning application is applied for ABB IRB 140 robot to find position deviations. The welding points in the chassis are divided into three areas to form the image processing algorithm and three image processing algorithms was created for each zone by using the NI vision assistant application. The points in the areas are found by image processing algorithm. For each area, the distance in the Z direction has been specified separately and the camera calibration parameters have been updated. Finally, the gas leakage test is performed to 500 products by using ABB IRB 140 robot in the production. The positions of seven welding points are collected according to test types which are the high-pressure test and the equilibrium test. Initially, the deviation values of the all welding points are figured separately on X and Y axis and the reasons for the deviations at the welding points are examined. Then, the descriptive statistics of deviations which are mean value, standard deviations, quartile, minimum and maximum values of deviations are given and the effect of the vision based positioning of ABB IRB 140 robot for the gas leakage test is shown.

The thesis organized in 6 sections including conclusion. In section 2, information about the ABB IRB 140 industrial robot used in the project has been given. The hardware structure, coordinate systems, kinematic and dynamic models, programming of the robot and implementation in PLC are explained. In Section 3, the image processing methods which are threshold, morphological operators and color plane extraction are used in image processing algorithm of gas leakage test and coordinate transformation and camera calibration methods are explained in detail. In section 4, describes the gas leak test station is explained and this section consists of

four subsections. Firstly, the operatorial logic and advantage of the heat pump dryer has been mentioned. Secondly, the purpose of the gas leak test and the operator and measurement logic are explained. Thirdly, the vision based positioning system which is used in the test station and the test cycle are presented. Finally, the generation image processing algorithms for divided three areas in the chassis for determining the position of the seven welding points. In Section 5, the camera used in experimental studies is explained and real-time experimental studies are presented. The deviations of position coordinates of welding points and presented and examined. Moreover, the mean, standard deviation, median, minimum and maximum values of deviations are examined for X and Y axis. Consequently, the results are concluded and discussed in the conclusion section.

2. ABB IRB 140 INDUSTRIAL ROBOT

An industrial robot is described as “an automatically controlled, can be programmable or reprogrammable into three or more axis or multipurpose manipulator, these are devices that are stationary or mobile for use in industrial automation practices. Moreover, they have the manipulator including actuators and the controller switch any communication interface and teach pendant” according to the ISO 8373:2012 [22]. The industrial robot types are determined by the number of joints and the type of joint. The abilities of industrial robots to manipulate the environment. The manipulators are machines that are composed of an segments of identifiable and concatenated identifiers and which are used to move objects in more than one degree of freedom. [23].

Six degrees of freedom (DOF) of ABB IRB 140 Robot which are three translational and three rotational DOF are used to oriented and positioned for an object. ABB IRB 140 that is uniformly distributed throughout the mechanical structure are sufficient for manipulation for objects in 3D space. However, robots with less six DOF can be used for many assignments, but their ability to position and orient objects is restricted. For example, robots with three translational DOF and one rotating DOF are sufficient for palletizing operators [24]. Palletizing robots are generally consisting of three prismatic joints and one rotational joint or only four rotational joints. An unlimited number of positions can be obtained before using too much six DOF to reach a certain position and orientation. In this context, unless a different definition is generally used, robot define an articulated arm with six revolute joints.

2.1 Hardware

ABB IRB 140 Robot has five main parts which are controller, arm, drive, gripper, sensor [25].

The controller is the "brain" of the industrial robotic arm and permits the parts of the robot to work together. It acts as a computer in the robot and permits the robot to also

be connected to other systems. The robotic arm controller runs program which is a set of instructions written in code. The program is inputted with a teach pendant. Many of today's industrial robot arms use an interface that resembles or is built on the Windows operating system [25]. The controller of ABB IRB 140 Robot is shown in Figure 2.1.

Figure 2.1 : The controller of ABB IRB 140 Robot.

The industrial robot arms have difference in shape and size. The part of the position of the industrial robot is end effector. The shoulder, elbow and wrist move with the robot arm and bend to place the end effector exactly at the right spot. The DOF of the robot is the number of these joints. The robots with three axis only move linearly: backward & forward, left & right and up & down. Six-axis robots must be used for rotational movements [26]. Most production plants use six-axis robots [26]. The industrial arms of ABB IRB 140 Robot with six-axis are shown in Figure 2.2.

The drive is the motor that moves the connections which are sections between joints to their specified positions. The types of drives which are hydraulic, electric and pneumatic are used largely for industrial robot arms. The hydraulic drive systems provide a robot great power and speed. An electrical system gives a robot to less speed and durability. Pneumatic drive systems are used for smaller robots with less motion axis. The drives must be periodically serviced and replaced if erosion begins [25].

Figure 2.2 : The ABB IRB 140 Robot.

The gripper is connected to the sixth axis of the robot. The gripper is a mechanical component that allows the hand to make direct contact with the components and to move with the robot. The grippers of the robots may differ in their tasks, and complex grippers may be programmed according to their functions. Some example applications are magnets, snipping tool, welding devices and vacuum pump [27]. In this study, HLD6000 Refrigerant Leak Detector is used as gripper for gas leak test is shown in Figure 2.3.

Figure 2.3 : The gripper of ABB IRB 140 Robot.

Sensors allow the industrial robotic arm to receive feedback about its environment. They can give the robot a limited sense of sight and sound. The sensor obtains data and sends it electronically to the robot controlled. One use of these sensors is to keep two robots that work closely together from bumping into each other. Sensors can also assist end effectors by adjusting for part variances. Vision sensors allow a pick and place robot to differentiate between items which is chosen and items which is ignored [28].

2.2 Coordinate Systems

2.2.1 Tool center point

The tool center point (TCP) is the point in relation to which all robot positioning is defined. In general, TCP is defined as the active point of the device used such as the center of gripper and the muzzle of a spot welding. The robot system can handle a few TCP definitions, but only one can be active at any one time. The TCP will be jogged or moved to the programmed target position. The tool center point also constitutes the origin of the tool coordinate system [29].

TCP will purse the actual track if the robot is programmed to go along a given track. Coordinate systems and the program of robot can be defined and moved according to other coordinate systems. The tool center point that is shown in Figure 2.4 is stated according to the coordinate system used in the program.

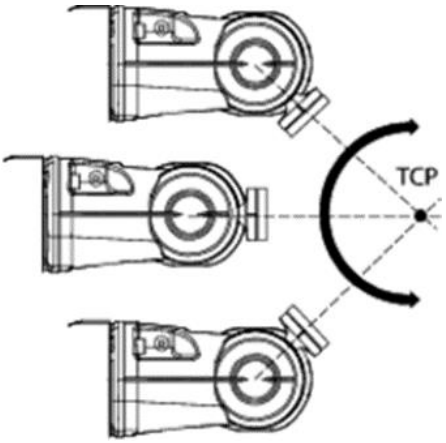

Figure 2.4 : The illustraion of tool center point.

TCPs have two basic types which are moveable and stationary. The moving TCP is used generally industrial applications and move with the flange of robot in the space. The measuring devices, the center of spot and arc welding gun which are added to

the robot tip, welding devices are examples of moveable TCP. Stationary TCP is defined as fixed TCP devices that are added to the fixed mechanism rather than to the end of robots. An example of this type of the stationary TCP is fixed spot welding gun.

2.2.2 Base coordinate system

The base coordinate system that is shown in Figure 2.5 is referenced to the base of the robot for fixed-mount robots. The center of the coordinate system is determined by the intersection of the 1st axis of the robot and the mounting surface. In the base coordinate system, the X axis is defined as the forward direction, the Y axis is defined as the left side of the robot, and Z axis is defined as the rotation axis. The base coordinate system for robot programming is the most appropriate choice for the other systems such as work object coordinate system [29].

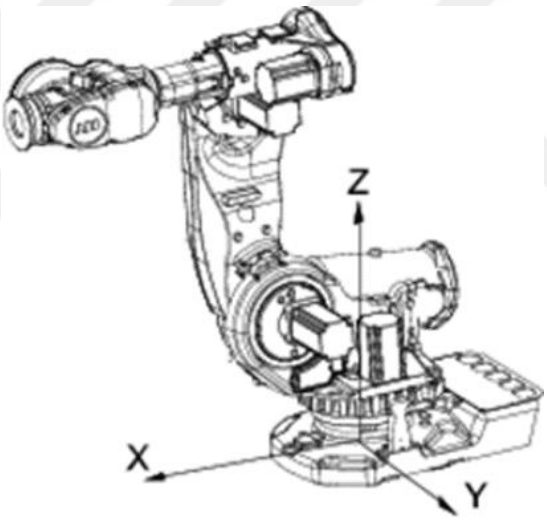

Figure 2.5 : The illustration of base coordinate system.

2.2.3 World coordinate system

The world coordinate system that is shown in Figure 2.6 has its zero point on a fixed position in the cell or station. The world coordinate system coincides with the base coordinate system by default. Especially if several robots work together, a world frame can be set up and the robots base coordinate systems can be expressed in relation to the world coordinate system. Therefore, this makes it useful for handling several robots or robots moved by external axis [29].

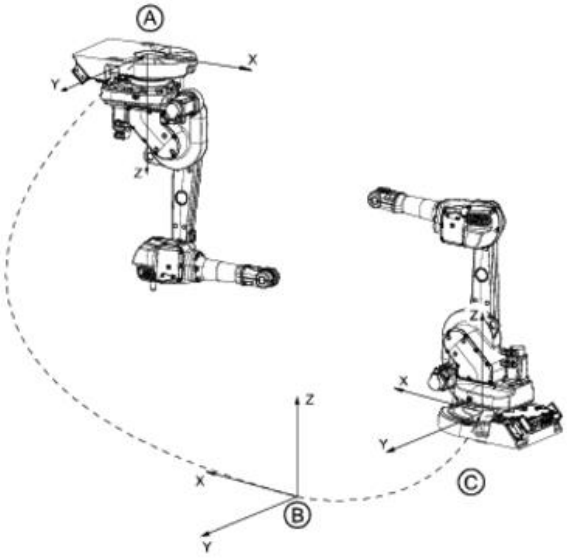

Figure 2.6 : The illustration of world coordinate system.

2.2.4 Work object coordinate system

The work object coordinate system which describes the position of the work tool associate to the world coordinate system corresponds to the work tool: The object frame (associate to the user frame) and the user frame (associate to the world frame) is used to define the work object coordinate system. Depending on the different work tools and the different positions of the same work tools, the robot can have various work object coordinate systems. The work tools may change positions in the work area. All targets and movements are updated simultaneously when the position change of work tool is defined in robot programming in the work object coordinate system is shown in Figure 2.7. This is one of the great advantages of working in the coordinate system.

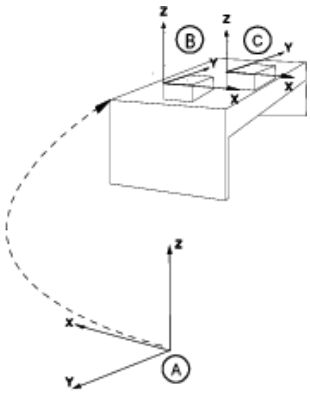

Figure 2.7 : The illustarion of work object coordinate system.

2.2.5 Tool coordinate system

A tool frame that is shown in Figure 2.8 is used to obtain information about the direction of the robot movement is required to define a TCP which is define the center of the tool coordinate system. The robot movements will be changed so that the new TCP will reach the target when the tool is changed. All robots have a predefined tool coordinate system, called tool0, located at the wrist of the robot. One or many new tool coordinate systems can then have defined as offsets from tool0.

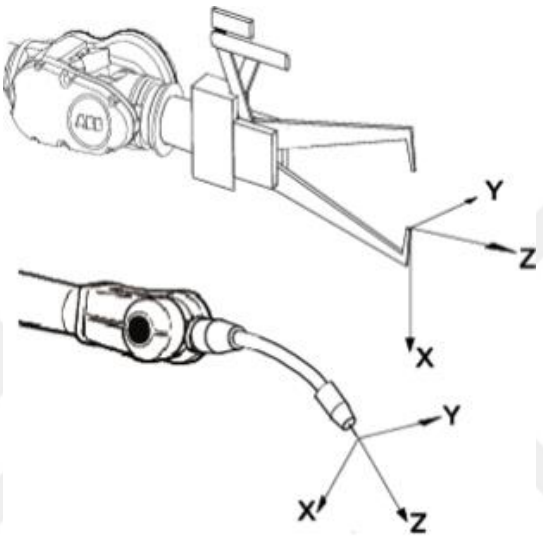

Figure 2.8 : The illustration of tool coordinate system.

2.3 Modeling

The first step of modelling of 6 DOF robot is the kinematics of robot. The motion of the joints without resorting to the strength that cause them is defined the robot kinematics. In this section, the forward and inverse kinematics of the IRB140 robot.

2.3.1 Kinematic modeling

The position of the manipulator given the joint positions is determined by using the forward kinematics. The definition of forward kinematics is made easier by knowing the DH parameters are given in [30] will be used in this study. The inverse kinematics allows determination of corresponding joint positions for the robot whose the actual and end effector pose is given. The same end effector pose can be reached in various configuration, corresponds to discrete joint position vectors. Therefore, the inverse kinematics problem is not one and has many solutions. It is widespread implementation to distinguish the inverse kinematics problem into two simpler

problems with the last three joints intersecting at a wrist for 6 DOF robots such as the IRB140 robot. The inverse position kinematics and inverse orientation kinematics is used for the definition of the inverse kinematic problem. problem. The Kinematic structure and frame assignments of the ABB IRB140 robot in Figure 2.9.

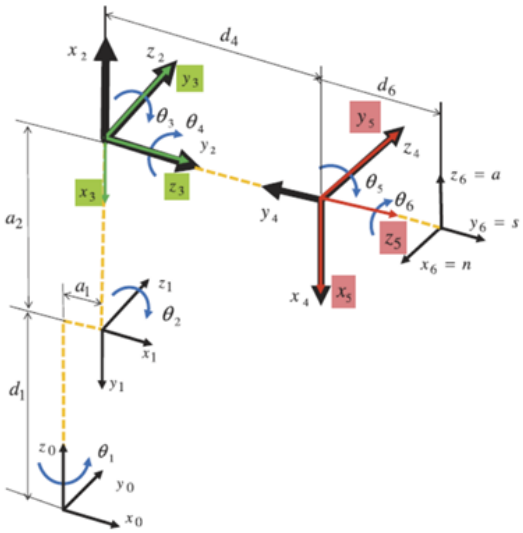

Figure 2.9 : Kinematic structure and frame assigments of the ABB IRB140 robot.

The Denavit–Hartenberg (DH) parameters of the IRB140 robot as described by [30] are shown in Table 2.1.

Table 2.1 : DH parameter of IRB140 robot

Axis	$\boldsymbol{\alpha_{i-1}}$	$\boldsymbol{a_{i-1}}$	$\boldsymbol{d_i}$	$\boldsymbol{\theta_{i-1}}$
1	0	0	d_1	θ_1
2	90	a_1	0	θ_2
3	0	a_2	0	θ_3
4	90	0	d_4	θ_4
5	-90	0	0	θ_5
6	90	0	d_6	θ_6

A geometrical solution for the inverse kinematics as derived by [31] is described as the Transformation matrix from sixth joint to first joint with respect to the base frame defines orientation of the end effector and the cartesian position as equation (2.1).

$$ {}^{6}_{0}T = \begin{bmatrix} r_{11} & r_{12} & r_{13} & P_{xw} \\ r_{21} & r_{22} & r_{23} & P_{yw} \\ r_{31} & r_{32} & r_{33} & P_{zw} \\ 0 & 0 & 0 & 1 \end{bmatrix} \tag{2.1} $$

where

$$
\begin{aligned}
r_{11} &= c_1c_{23}(c_4c_5c_6 - s_4s_6) - c_1s_5s_{23}c_6 + s_1(s_4c_5c_6 + c_4s_6) \\
r_{12} &= -c_1c_{23}c_4c_5c_6 + c_1s_{23}s_5s_6 - s_1s_4c_5c_6 \\
r_{13} &= c_1c_{23}c_4s_5 + c_1s_{23}c_5 + s_1s_4s_5 \\
r_{21} &= s_1s_{23}(c_4c_5c_6 - s_4s_6) - s_1s_{23}s_5c_6 - c_1(s_4c_5c_6 + c_4s_6) \\
r_{22} &= -s_1c_{23}c_4c_5c_6 + s_1s_{23}s_5s_6 - c_1s_4c_5c_6 \\
r_{23} &= s_1c_{23}c_4c_5c_6 + s_1s_{23}s_5 - c_1s_4s_5 \\
r_{31} &= s_{23}(c_4c_5c_6 - s_4s_6) + c_{23}s_5c_6 \\
r_{32} &= -c_6s_{23}c_4c_5 - c_{23}s_5s_6 \\
r_{33} &= s_{23}c_4c_5 - c_{23}c_5 \\
P_{xw} &= c_1s_{23}d_4 + c_1c_2a_2 + c_1a_1 \\
P_{yw} &= s_1s_{23}d_4 + s_1c_2a_2 + s_1a_1 \\
P_{zw} &= -c_{23}d_4 + s_2a_2 + d_1
\end{aligned}
\tag{2.2}
$$

The position of the wrist center is defined as P_{xw}, P_{yw} and P_{zw}.

The solution for first angle q_1 from Figure 2.10 become as equation (2.3).

$$
q_1 = \text{atan}(P_{yw}, P_{zw}) \tag{2.3}
$$

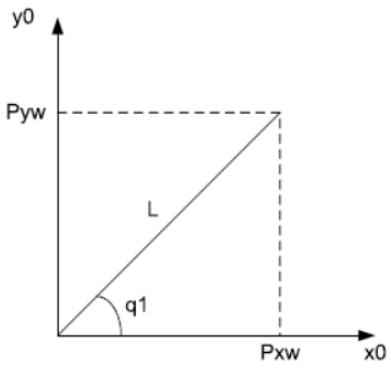

Figure 2.10 : Projection of the wrist center onto the xy plane.

The expressions for the other joints q_2 to q_6 become as equations (2.4, 2.5, 2.6, 2.7, 2.8).

$$
\begin{aligned}
q_2 = \text{atan}(P_{zw} - d_1, &\sqrt{P_{xw} + a_1\cos(q_1^2) + \left(P_{yw} + a_1\sin(q_1)\right)^2} \\
&- a\tan(d_3\sin(q_3), a_2d_4\cos(q_3))
\end{aligned}
\tag{2.4}
$$

$$
q_3 = \text{atan}\left(\mp\sqrt{(1 - D^2}, D\right) \tag{2.5}
$$

$$q_4 = atan(s_1 r_{13}, c_1 r_{23}, c_1 c_{23} r_{13} + s_1 c_{23} r_{23} + s_{23} r_{33}) \tag{2.6}$$

$$q_5 = atan(c_1 c_{23} c_4 + s_1 s_4)\, r_{13} + (s_1 c_{23} c_4 - c_1 s_4) r_{23} + s_{23} c_4 r_{33}, \\ (c_1 s_{23}) r_{13} + (s_1 s_{23}) r_{23} - c_{23} r_{33} \tag{2.7}$$

$$q_6 = atan(-c_1 c_{23} s_4 + s_1 c_4)\, r_{11} - (s_1 c_{23} s_4 - c_1 c_4) r_{21} - s_{23} s_4 r_{31}, \\ (-c_1 s_{23} s_4 + s_1 c_4) r_{12} - (s_1 s_{23} s_4 + c_1 c_4) r_{22} - s_{23} s_4 r_{32} \tag{2.8}$$

2.3.2 Dynamic modeling

The Euler-Lagrange method which approach is energy based and the Newton-Euler method which investigate the forces between each of the links in a iterative manner exist for dynamic modelling of industrial robots with n degrees of freedom. Compared to these two methods, the Newton-Euler method was found to provide a faster and more accurate model for modeling higher degree of freedom robots. In this study, The Newton-Euler method is used in dynamic modeling because this method that is more suitable described as equation (2.9).

$$M(q)\ddot{q} + \mathrm{C}(\mathrm{q}, \dot{\mathrm{q}}) + \mathrm{G}(\mathrm{q}) = K(q, \dot{q})u \tag{2.9}$$

where $q(t) \in R^n$ is the vector of angular joint positions called as the generalized coordinates. $u(t) \in R^n$ are forces driving the joints and the control inputs. $M(q)$ is a positive definite nxn rotatable matrix reflecting the inertia forces [32]. $C(q, \dot{q})$ is an n dimensional vector of centrifugal and Coriolis terms and $G(q)$ is an n dimensional reflecting the gravitational forces. $K(q, \dot{q})$ is the matrix characterizing the actuating forces. For n-DOF robot, it is also supposed that $\dim(q) = \dim(u)$ and $\dim(q) = \dim(u)$.

In order to facilitate representation for smoothness analysis it is important to express it in a nonlinear form the Equation 2.9. The equation becomes in the form as equation (2.10).

$$\dot{q} = \mathrm{f}(\mathrm{q}, \mathrm{u}) \tag{2.10}$$

The Equation 2.10 has six second order differential equations for a 6-DOF robot. This equation can be converted to twelve first order differential equations. The equation 2.11 becomes as equation (2.11).

$$
\begin{aligned}
x_1 = q_1\, x_1 = \dot{q_1} \\
x_2 = q_2\, x_2 = \dot{q_2} \\
\vdots \\
x_5 = q_5\, x_5 = \dot{q_5} \\
x_6 = q_6\, x_6 = \dot{q_6}
\end{aligned}
\tag{2.11}
$$

The equation 2.12 becomes the first order form as equation (2.12).

$$
\begin{aligned}
\dot{x}_1 = \mathrm{x}_7\dot{\mathrm{x}}_7 = \mathrm{f}_7(x,u) = \ddot{q}_1 \\
\dot{x}_2 = \mathrm{x}_8\dot{\mathrm{x}}_8 = \mathrm{f}_8(x,u) = \ddot{q}_2 \\
\vdots \\
\dot{x}_6 = \mathrm{x}_{12}\dot{\mathrm{x}}_{12} = \mathrm{f}_{12}(x,u) = \ddot{q}_6
\end{aligned}
\tag{2.12}
$$

The equation 2.13 becomes in stated space is now of the form as equation (2.13).

$$
\dot{x} = \mathrm{f(x)} + \mathrm{g(x)u} \tag{2.13}
$$

and the output vector in the equation 2.14 becomes as equation (2.14).

$$
y = \mathrm{h(x)} \tag{2.14}
$$

$f(x)\colon R^{2n} \rightarrow , g(x)\colon R^n \rightarrow R^{2n}$. f refers R^n to R^{2n}, g is smooth matrix function and h is smooth function. It is seen that functions can be continuously distinguished enough times. The Equation 2.15 defines these vectors as equation (2.15).

$$
\begin{aligned}
f(x) &= \begin{bmatrix} x_2 \\ M(x_1)^{-1}\left(-C(x_1,x_2)x_2 - G(x_1)\right) \end{bmatrix} \\
g(x) &= \begin{bmatrix} 0_{nxn} \\ M(x_1)^{-1} \end{bmatrix}
\end{aligned}
\tag{2.15}
$$

In the Equation 2.15, twelve states describe a system with a variable second order. The outputs to be controlled are a vector of the common axis of the robot becomes as equation (2.16).

$$
y = h(x) = Cx \tag{2.16}
$$

where C is a matrix defined by $C = [I_{nxn}\ 0_{nxn}]$.

2.4 Programming and PLC implementation

The essential overview of the robot control system is shown in Figure 2.11. The robot needs commands to control the robot arms. These commands are programmed by the user in the high-level programming language RAPID for ABB robots. High level program language means that the program is quite user friendly.

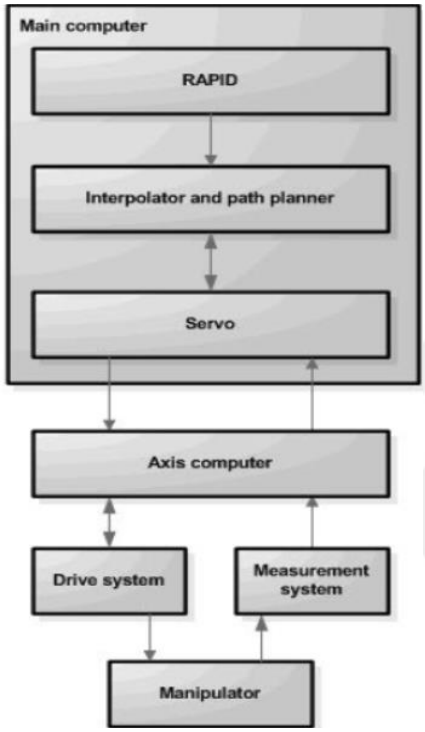

Figure 2.11 : The overview of robot control.

The flex pendant that is a hand control connected to a computer to is used for controlling manually the ABB robots. A robot program is programmed in the RAPID program language for the ABB robots that tells the robot how to move and which way to go the robot. There are two methods of writing Rapid programs. The first method is the program can be written directly on flex pendant. The other method is the program can be written in the PC environment and can transfer the board of the robot from the computer using USB connection and TCP-IP connection [33].

The RobotStudio is a Graphical User Interface (GUI) is used for the ABB robots for offline programming, modelling and configuration. The programmer can be simulated robot execution a RAPID program in the drawing environment by the help of Robot virtual technology [34]. The CAD files can then be transferred and added to the robot or work cell. The offline simulation that is synchronized with a Virtual

Controller (VC) can be designed in the RAPID program to observe the movements of the robot. With offline simulation, the robot can be tested for accessibility for roads and targets in the work area, and can be debugged in the robot program before the program is loaded. The programmer can program the robot directly via flex pendant or load the program he has written via RobotStudio or any movable appliance like USB. The robot manipulator is controlled by the functions available with the IRC5 (Industrial Robot Controller), which consists of the control module and the drive module. The power electronics is created the software, the memory and the operating system [35].

In this thesis, the program of ABB IRB 140 Robot is implemented to Programming Logic Controller (PLC) in the automatic test station consists of three devices: camera with controlling PC module, PLC and ABB IRB 140 robot. The PLC allows the two other devices to work together, transfer the position data from the camera to the robot, and separate the product from the test according to the test completion data taking from ABB IRB 140 Robot. The total test time is around 15 seconds. For this reason, PLC controls take over to complete the process quickly.

The use of a ABB IRB 140 Robot is due to the presence of leaks at the welding points thanks to the gas leak measurement detector located at the end of the intended robot. The robot should communicate with the camera in the test station because the position of the source points at the leak points may change. If the communication is incomplete, it may happen that the source point is not found and the test is not successful.

The communication network using the Profinet communication protocol between camera, robot and PLC is shown in Figure 2.12.

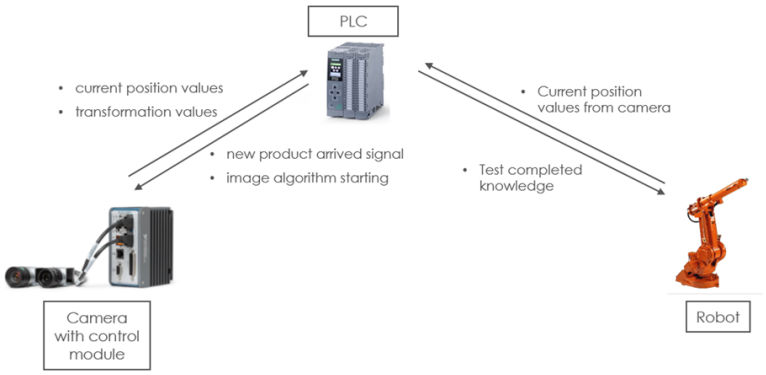

Figure 2.12 : Communication network of test station.

PLC is main controller in test automation systems handling all assignments beside the robot moves to the positions taken after the end of image processing. Profinet communication is chosen to communicate between PLC - ABB IRB 140 Robot and PLC- camera with control module. The PLC receives the information of the product coming to the test station and commands the camera to take a picture of the product to be tested and commands the position of the welding points after the image processing process to be obtained. Coordinate transformations are performed on the positions taken by the image processing and position data are sent to the robot by the PLC. Robot test start and test completion signals are provided by the PLC. In addition, the PLC gives the command to continue the production line on completion of the test.

The controller is Siemens S1200 and programming environment is “TIA Portal”. A sample screen from implementation of the program is shown in Figure 2.13.

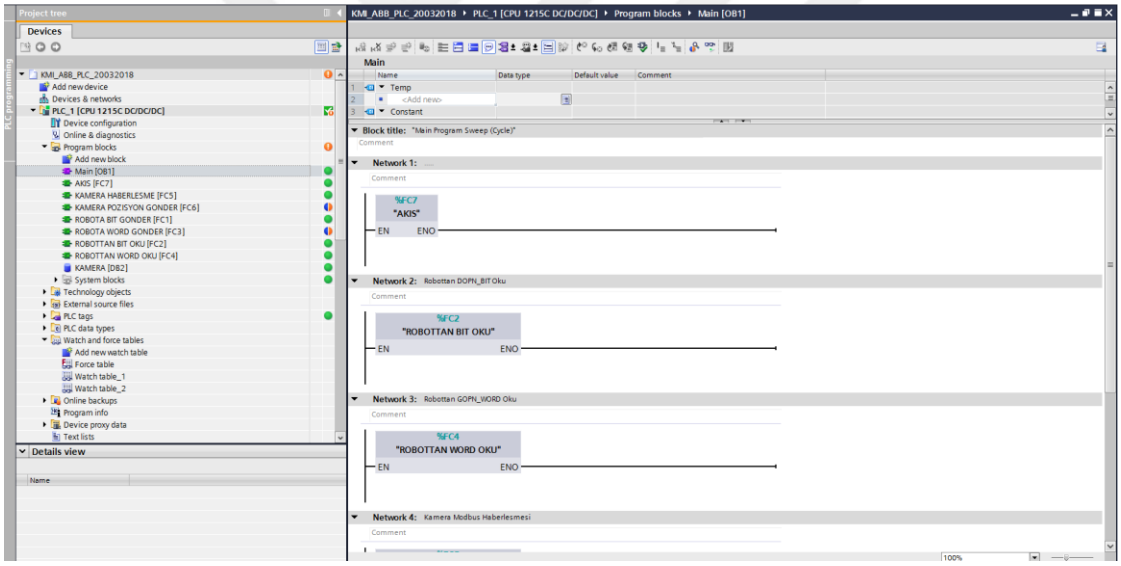

Figure 2.13 : PLC program structure of test station.

3. IMAGE PROCESSING METHOD AND CAMERA CALIBRATION

Image processing is a method used to apply some procedures on an image and obtain an enhanced image or extract some useful information from it. It is a signal processing type in which the input is an image and output is an image or feature / property associated with this image. Today, image processing is one of the main research topics in engineering and computer science and is the most widely used method among technological methods [36].

Image processing involves essentially the following three steps:

- Importing the image into image acquisition tools
- Examination and handling the image
- Obtaining the outputs can be a result of the processed photo and the report of image processing analysis.

Analogue and digital image processing are two type of methods are used for image processing. Analog image processing can be used for printed copies such as printouts and photographs. Various interpretation is used by image analysts while using these visual techniques. Digital image processing techniques help to manipulate digital images using a computer. The purpose of digital image processing is to produce useful information from images without human assistance [37]. Some of the digital image processing techniques which are threshold, morphological operators, and color plane extraction that will be used in this study will be described.

3.1 Threshold

One of the simplest method of image processing is thresholding can be used to generate binary image from a gray scale image. Binary images are generated by using segmentation which is the process of appointing each pixel two or more classes in the source image from color images. The purpose of using the threshold method is to divide into smaller segment or associations using at least one color or gray scale

value to constrain the intended image in the image processing. Reducing the process of classification and recognition and simplifies the complexity of the data are benefits of obtaining a binary image [38].

The most common method to convert a gray image to a binary image is to select a single threshold value [39].

In the simplest implementation, a gray scale of color image is the input of thresholding operator and a binary image is the output of thresholding. In thresholding operator, foreground is expressed by white pixels and background is expressed by black pixels. The equations of foreground pixel and background pixel becomes as equation (3.1).

$$g(x,y) = 1 \;\; if \; f(x,y) \; is \; foregorund \; pixel$$
$$g(x,y) = 0 \;\; if \; f(x,y) \; is \; backgroun \; pixel \tag{3.1}$$

All pixels are applied single fixed criterion simultaneously for this segmentation method in the image [40].

In real practical applications, histograms are more complex with many peaks and open valleys, and choosing the T value is not always easy. The equation for more complex applications becomes as equation (3.2).

$$g(x,y) = \left[\frac{0 \; f(x,y) < T}{1 \; f(x,y) => T}\right]$$
$$T = T\,[x, y, p(x,y), f(x,y)] \tag{3.2}$$

where $p(x,y)$ is some local property and $f(x,y)$ is the gray level. If $f(x,y)$ is bigger than T, the point is represented as an object point. On the other hand, the point is represented a background point [41].

3.2 Morphological Operator

The morphological operators are used easily and most of them are mainly logical operators although the morphological operators are based on set theory [42]. Dilation and erosion are the essential morphological operators and opening and closing are other operators.

3.2.1 Dilation operator

Dilation operator enlarges an object by its size. The extent to the growth based on the shape and nature of the structuring element. The dilation of an image A(set) by structuring element B is becomes as equation (3.3).

$$A \oplus B = \{z | \widehat{(B)_z} \cap A \neq \emptyset \tag{3.3}$$

The dilation of A by is the set of all displacements z so B' and A consist at least one common element because of the set B is reflected in relation to its origin and shifted by z. The dilation extends the number of white pixels with value one (foreground), in other words the dilation makes addition pixels to the boundary elements. Conversely, the number of black pixels with value zero (background) are decreased in the dilation.

The holes in the continuous objects are filled fundamentally with this dilation process. In the dilation operator, as the joints are made to the boundaries of the object, the intensity of the object's position influences and the effect of blurring can be observed. Therefore, this operator likes analogous to smoothing spatial low pass filters which are applied in linear filtering of the image. The situation before and after the application of the dilation operator is shown in Figure 3.1.

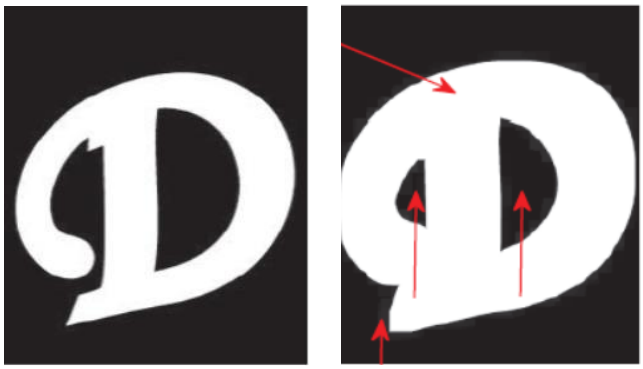

Figure 3.1 : The effect of dilation operator.

3.2.2 Erosion operator

The erosion operator is complementary to the dilation process with the operator effect. Erosion operator shrinks an object by its size. The erosion of an image A(set) by structuring element B is becomes as equation (3.4).

$$A \oplus B = \{z | \widehat{(B)_z} \cap A \neq \emptyset \tag{3.4}$$

The erosion of image A according to structure B is the set of all points z, such that the construction element B is a subset of the view, which is translated by z. The erosion extends the number of black pixels with value zero (background), in other words the erosion decreases pixels to the boundary elements. Conversely, the number of white pixels are increased in the erosion.

The erosion is used to remove the noisy connection between two objects because the structures are smaller than the whole structure are subtracted in the erosion process. In the erosion operator, the unwanted pixels are removed thus the effect of sharpening can be observed. Therefore, this operator likes analogous to sharpening high pass filters which are applied in linear filtering of the image. The situation before and after the application of the erosion operator is shown in Figure 3.2.

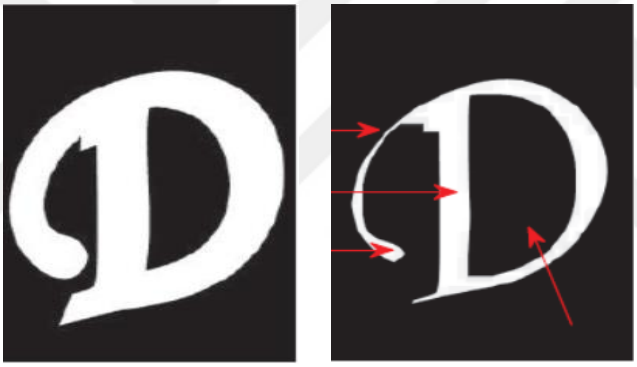

Figure 3.2 : The effect of erosion operator.

3.2.3 Opening operator

Opening operator is formed by the combination of erosion and dilation. The relationship between opening, erosion and dilation is given following equation. The opening of an image A (set) by structuring element B is becomes as equation (3.5).

$$AoB = (A \ominus B) \oplus B \tag{3.5}$$

The opening operator is occurred sequentially that the erosion of an image by structuring element and the outcome is dilated with the identical structuring element. The boundary of the opened image which attains the extreme points of A and B boundary is rolled around inside of this boundary. It is the points in the structuring B element.

Minor extensions presents are removed, the narrow bridges are erased and the outline of an object are become smooth in the object by using the opening operator. The situation before and after the application of the opening operator is shown in Figure 3.3.

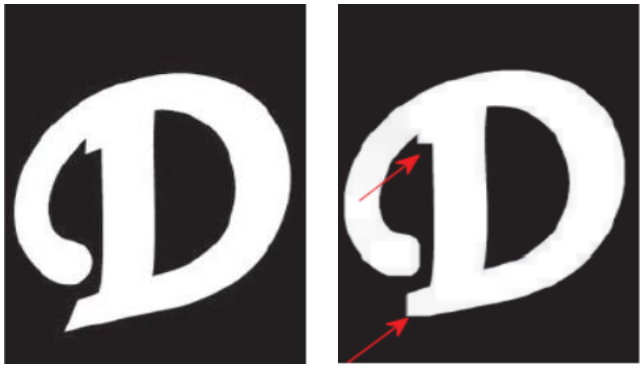

Figure 3.3 : The effect of opening operator.

3.2.4 Closing operator

Closing operator is formed by the combination of erosion and dilation. The relationship between opening, erosion and dilation is given following mathematical statement. The difference between the opening operator of closing operator is that the sense of order of occurrence of erosion and dilation operator. The opening of an image A (set) by structuring element B is becomes as equation (3.6).

$$AoB = (A \oplus B) \ominus B \tag{3.6}$$

The closing operator is occurred sequentially that the dilation of an image by structuring element and the outcome is eroded with the identical structuring element. The boundary of the closed image which attains the extreme points of A and B boundary is rolled around outside of this boundary. It is the points in the structuring A element.

Blend narrows are cut, gaps blanched and the sections of contours are become smooth in the object by using the closing operator. Consequently, small holes are removed and gaps are filled in the object boundaries. The situation before and after the application of the closing operator is shown in Figure 3.4.

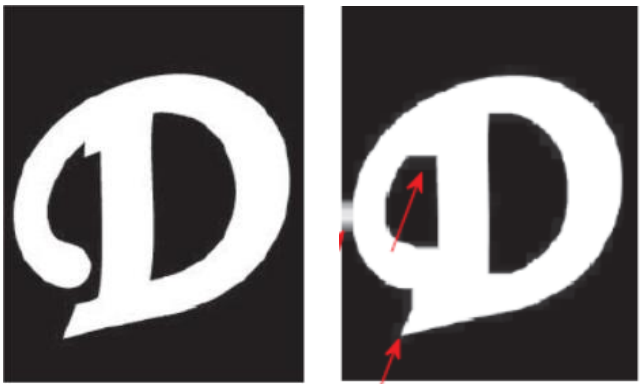

Figure 3.4 : The effect of closing operator.

3.3 Color Plane Extraction

The color information in images are included by color plane extraction. The background and foreground color of each image has different values according to Red Green Blue (RGB) values. The compensation for cross-color blending in the color filter provides with RGB color correction [43]. The equation (3.7) becomes as a set of matrix coefficients (a_i, b_i, c_i) in the matrix calculations. Moreover, the matrix parameters must correspond the equality in the equation (3.8) because the matrix is indicated is not enough to correct the entire color space.

$$\begin{bmatrix} R' \\ G' \\ B' \end{bmatrix} = \begin{bmatrix} a_1 & a_2 & a_3 \\ b_1 & b_2 & b_3 \\ c_1 & c_2 & c_3 \end{bmatrix} \begin{bmatrix} R \\ G \\ B \end{bmatrix} \tag{3.7}$$

$$\sum_{i=1}^{3} a_i = \sum_{i=1}^{3} b_i = \sum_{i=1}^{3} c_i = 1 \tag{3.8}$$

Color-oriented quality in the corrected image is obtained to increase the main diagonal values. RGB has two advantages which are better light sensitivity due to reduction of light loss and color representation characteristics compare to complementary color filter array [44].

3.4 Camera Calibraition

3.4.1 Basic camera model

All light rays from a exact object point to a single point is converted by the lens in the camera in the image plane. If the lens is weak, distortion may be neglected, lens law become as equation (3.9).

$$\frac{1}{\propto}+\frac{1}{\beta}=\frac{1}{f} \tag{3.9}$$

where $\propto$ represents the distance between the lens and the object, β represents the distance between the lens and the image plane and f represents is the local length. The lens law is shown in Figure 3.5.

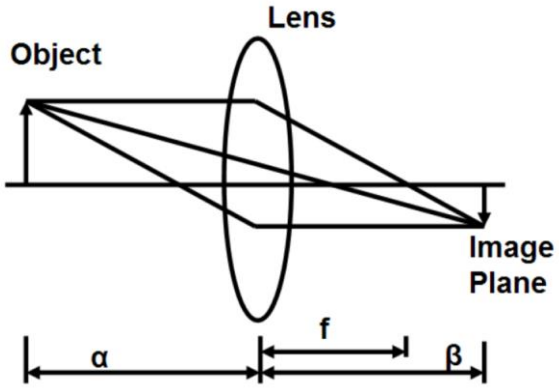

Figure 3.5 : The illustration of lens law.

In the image plane, an object has distance $\propto$ from the lens will be reproduced with full sharpness by the lens law. The reproduction will be more or less blurred because the difference between the object and the object is different $\propto$ in the image plane. The depth of field called as s how blurred the image will be becomes as equation (3.10).

$$s = 2\lambda\left(\frac{f}{D}\right) \tag{3.10}$$

where λ is the wavelength of incoming light and D is the diameter of the gap. The depth of field can also be described as the resolution of interval is greater than $\frac{1}{2d}$ where the resolution $\frac{1}{d}$. The equation 3.11 becomes as equation (3.11).

$$\frac{1}{d} = \frac{1}{\lambda}\left(\frac{D}{f}\right) \tag{3.11}$$

3.4.2 Pinhole camera model

The actual lens care is reflected accurately and the radial lens distortion and tangential distortion are introduced by using the pinhole camera model.

The several coordinate systems is shown in Figure 3.6. $P(X, Y, Z)$ represents world coordinate systems, $P_C\ (X_C, Y_C, Z_C)$ represents camera coordinate systems, $P(x, y)$ represents physical coordinate systems and, $P(u, v)$ represents pixel coordinate systems in the Figure 3.6. The purpose to convert a 3 dimensional $point\ P_W\ (X_W, Y_W, Z_W\ )$ in world coordinate systems into a point $P(u, v)$ in image pixel coordinate systems can be obtained in four steps [45].

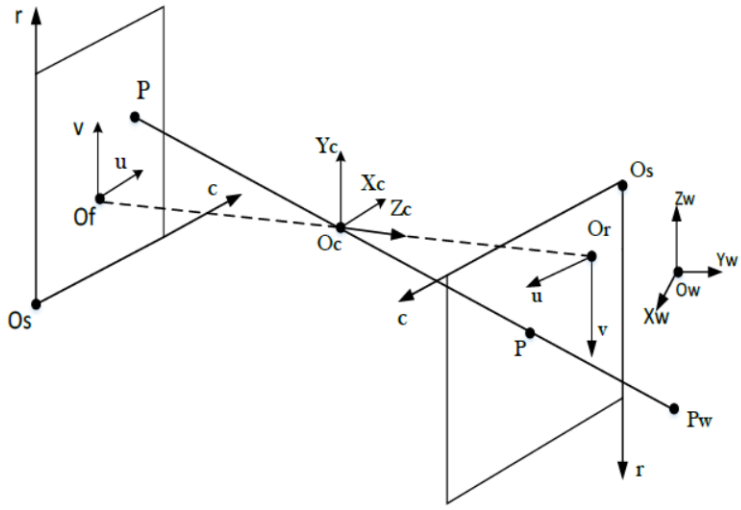

Figure 3.6 : The coordinate systems of pinhole camera model.

The first step is the camera coordinates $P_C\ (X_C, Y_C, Z_C)$ becomes according to the world coordinates $P(X, Y, Z)$ as equation (3.12).

$$P_C = \begin{pmatrix} R & T \\ 0 & 1 \end{pmatrix} P \tag{3.12}$$

where R is $3x3$ rotational matrix and T is a $3x1$ translation vector.

The second step is the physical coordinates $P(x, y)$ in the image plane coordinate systems obtains for projection of the camera coordinates $P_C\ (X_C, Y_C, Z_C\ )$ in pinhole model becomes as equation (3.13).

$$\begin{pmatrix} x \\ y \end{pmatrix} = \begin{pmatrix} X_c/Y_c \\ Y_c/Z_C \end{pmatrix} P \tag{3.13}$$

The third step is the correction of $P_{C0}\,(X_{C0}, Y_{C0}, Z_{C0})$ to extent the physical coordinates $P(x, y)$ by presenting the radial lens distortion and tangential lens distortion becomes as equation (3.14).

$$\begin{pmatrix} u \\ v \end{pmatrix} = \begin{pmatrix} f_x x_q + c_x \\ f_y y_q + c_y \end{pmatrix} \tag{3.14}$$

where f is the effective focal length of camera, (c_x, c_y) represents in the base point.

Finally, the corresponding equation can be obtained as equation (3.15).

$$s.p = A(R|t)P \tag{3.15}$$

where $P = (X, Y, Z, 1)^T$ represents the homogeneous coordinates in the space, $(R\,|\,t)$ represents the external parameters matrix, A is seen that the internal parameter matrix and $p = (u, v, 1)^T$ represents homogeneous coordinate in the image pixel coordinate system.

3.4.3 Coordinate transformation

In the Figure 3.6, the image coordinate system is represented by r, c, O_s , the image plane coordinate system u, v, O_f, the camera coordinate system is represented by X_c, Y_c, Z_c, O_c the world coordinate system is represented by X_w, Y_w, Z_w, O_w [46].

One point in the world coordinate system is P_w. Firstly, this point is transformed in to the camera coordinate system with two operators that are rotation and translation. The equation (3.16) become as the translation between $P_w = (X_w, Y_w, Z_w)^T$ and $P_C = (X_C, Y_C, Z_C)^T$.

$$P_c = R\,P_w + T \tag{3.16}$$

The point in the camera coordinate system $P_C = (X_C, Y_C, Z_C)^T$ projected onto the point $P = (u, v)^T$ in the image coordinates is parallel projection. The equation (3.17) becomes as the projection relations.

$$\begin{pmatrix} u \\ v \end{pmatrix} = m \begin{pmatrix} x_c \\ y_c \end{pmatrix} \tag{3.17}$$

where m is the magnification. The equation (3.18) becomes as the definition of magnification.

$$m = \frac{f}{x_z} \tag{3.18}$$

where f is the focal length and x_z is the distance from the point to the lens on the z direction.

The point in the image plane coordinate system is represented as $(r, c,)^T$ is defined in the equation (3.19).

$$\begin{pmatrix} r \\ c \end{pmatrix} = \begin{pmatrix} \frac{v}{S_y} + C_y \\ \frac{u}{S_x} + C_x \end{pmatrix} \tag{3.19}$$

where S_x and S_y are the scaling factor, C_x and C_y are the coordinate values of corresponding points of the origin of the imaging plane coordinate system in the image plane coordinate system.

3.4.4 Application of camera calibration

The optical axis of the working area is perpendicular to each other in the automatic probe positioning system. Thus, the rotation matrix R can be set in the camera calibration process as equation (3.20).

$$R = \begin{pmatrix} \cos\alpha & -\sin\alpha & 0 \\ \sin\alpha & \cos\alpha & 0 \\ 0 & 0 & 1 \end{pmatrix} \tag{3.20}$$

The following equalities in equation (3.21) are obtained by the equation (3.16) and the equation (3.20).

$$x_w = Ar + Bc + C$$

$$y_w = Dr + Ec + F$$

$$A = -ms_y \sin\alpha_i\,, \quad B = ms_x \cos\alpha_i$$

$$C = -ms_x \cos\alpha + ms_y c_y \sin\alpha + t_1 \tag{3.21}$$

$$D = ms_y \cos\alpha\,, \quad E = ms_x \sin\alpha$$

$$F = -ms_x c_x \sin\alpha - ms_y c_y \cos\alpha + t_2$$

Hence, camera calibration process is converted in the process of order converts camera calibration process to find the six parameters.

In this study, the grid partition which is shown in the Figure 3.7 is used for camera calibration. The points form the world coordinate of ABB IRB 140 robot are selected on the grid partion. The parameters are selected as $\frac{f}{5{,}6} = 13{,}4$, $x_z = 220\ mm$, $S_x = 1628\ px$ and $S_x = 1236\ px$.

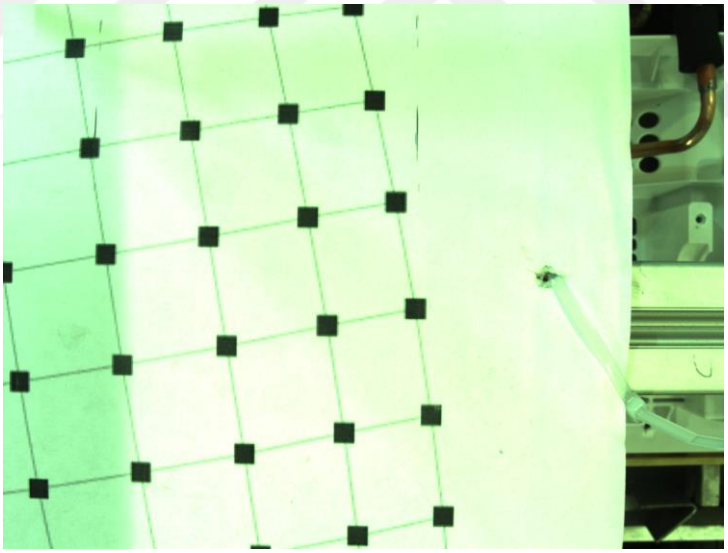

Figure 3.7 : The grid partition on the world coordinate system

For the solution of camera calibration parameters,15 points have been chosen. These points have values in the world coordination of ABB IRB140 robot $P_{wi} = (X_{wi}, Y_{wi}, Z_{wi})^T, i = 1{,}2{,}3, \dots, 15$ and image coordinate system $P_i = (u_i, v_i)^T, i = 1{,}2{,}3, \dots, 15$.

$$P_w = \begin{pmatrix} 265 & 115{,}7 \\ 269{,}1 & 144{,}8 \\ 241{,}6 & 122{,}46 \\ 245{,}8 & 151{,}9 \\ 215{,}4 & 129{,}96 \\ 218{,}7 & 159{,}39 \\ 241{,}99 & 179{,}97 \\ 265{,}46 & 172{,}9 \\ 209{,}03 & 99{,}36 \\ 237{,}4 & 94{,}03 \\ 261{,}35 & 87{,}94 \\ 260{,}81 & 201{,}5 \\ 204{,}49 & 71{,}08 \\ 231{,}83 & 65{,}94 \\ 186{,}2 & 135{,}32 \end{pmatrix}, \; P = \begin{pmatrix} 900 & 455 \\ 946 & 696 \\ 705 & 487 \\ 752 & 734 \\ 476 & 531 \\ 516 & 783 \\ 783 & 969 \\ 984 & 934 \\ 425 & 293 \\ 659 & 258 \\ 850 & 226 \\ 1010 & 1164 \\ 397 & 72 \\ 609 & 40 \\ 243 & 571 \end{pmatrix}$$

The least square method is used to find camera calibration parameter with the objection function in the equation (3.22).

$$\begin{aligned} f_1(A,B,C) &= \sum (A\, r_i + B\, c_i + C - x_{wi})^2 \\ f_2(D,E,F) &= \sum (D\, r_i + E\, c_i + F - y_{wi})^2 \end{aligned} \tag{3.22}$$

The new version of the objective function in the equation (3.23). was obtained after the expansion of the objective function and simplification and derivation of the unknowns.

$$\begin{cases} A\sum r_i + B\sum c_i + n\,C - \sum x_{wi} = 0 \\ A\sum r_i^2 + B\sum r_i\, c_i + C\sum r_i - \sum r_i\, x_{wi} = 0 \\ A\sum r_i\, c_i + B\sum c_i^2 + C\sum c_i - \sum c_i\, x_{wi} = 0 \end{cases}$$
$$\begin{cases} D\sum r_i + E\sum c_i + n\,F - \sum y_{wi} = 0 \\ D\sum r_i^2 + E\sum r_i\, c_i + F\sum r_i - \sum r_i\, y_{wi} = 0 \\ D\sum r_i\, c_i + E\sum c_i^2 + F\sum c_i - \sum c_i\, y_{wi} = 0 \end{cases} \tag{3.23}$$

The parameters are found as $A = 3{,}46$, $B = 2{,}29$, $C = 93{,}88$, $D = 0{,}74$, $E = 0{,}43$, $F = 20{,}88$. Consequently, the camera calibration is achieved.

4. GAS LEAKAGE TEST STATION

4.1 Heat Pump Dryer

The dryer which is shown in Figure 4.1 contains a drum clothes to be dried and a system for equipping heated dry air at initial temperature to the drum. The air supply system includes an air flow path having a heat pump (HP) evaporator for lowering the temperature of the air below the raw point temperature and removing air from the air leaving the room. The HP air system is also used to raise the temperature of the air from the evaporator to the first temperature [47]. The advantages of HP dryers are consuming less energy than other drying systems, providing a higher energy class and less damage to clothes [48].

Figure 4.1 : The heat pump dryer.

The chassis of HP dryer, in which gas leak control automation will be applied, contains compressor, condenser, evaporator, copper pipe. It is shown in Figure 4.2.

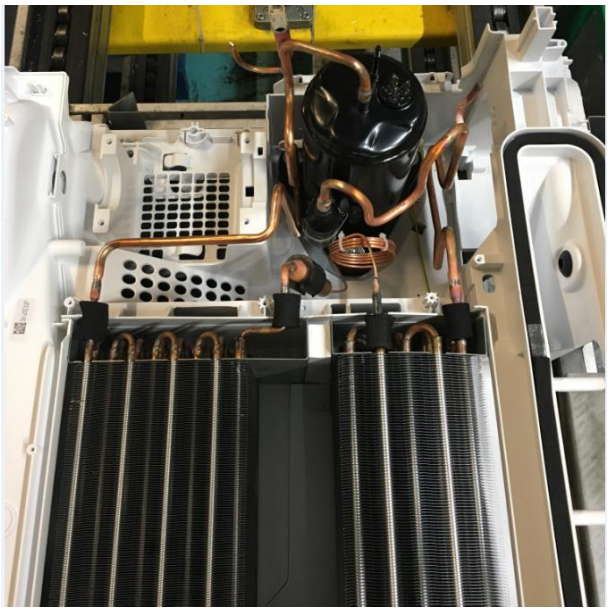

Figure 4.2 : The chassis of heat pump dryer.

The purpose of HP dryer is to prohibit the relative humidity enhancement in the drying air by taking some amount of environmental air through the settling flaps. The system air mixed with the environmental air should allow the relative humidity to maintain the required values in order to maintain the moisture content, rather than dehumidify on the cold surface. Otherwise, the environmental air should allow for the evaporator of the rising air by relative humidity drying in climatic conditions where the relative humidity level is low [49]. The drying air, relative humidity and temperature should be adjusted to the system through the drying drum inlet after the measurement and adjustable flaps and air volume to be emptied from the system in the HP dryer. The reduction of the relative humidity is achieved without lowering the temperature of the drying air with this arrangement. The front surface of the drying chamber was constructed with double-glazing to control the mass change in the dryer, for this reason, the interior volume is made visible [50].

4.2 Gas Leakage Test

A gas leak detection system for the detection and monitoring of HP dryer systems, controls, manages and monitors the dryer systems. The system includes a gas leak detector and a monitor and relay system to detect the presence of gas present in the compressor and evaporator units, assess the magnitude of the problem and assess the magnitude of the problem, alert operators and quality personnel [51]. Emergency shutdown means repairs to the system and shutting down the system until the system

is reset, meaning that if a significant hot air leak is detected, the drying system will shut down and store the contents.

In this thesis, the purpose of the gas leak is that control the sealing of the products manufactured in the production line by the acetylene welding method of the compressor, evaporator, condenser and copper pipe groups to each other. Every product is manufactured in the production line is checked for leaks in the test station. Leakage is measured in years/gram. The products are pressed in gas at a 300 minimum gram to a maximum gram of 500. The gas in the compressor passes first through the condenser, then through the copper pipes, passes through the evaporator, and then returns to the compressor again. The gas leakage is measured at the weld points of the gas passing through the copper pipes. In principle, two types of gas leakage measurements are made. 7 welding points controlled in both tests are shown in the Figure 4.3. The source points marked with blue are high pressure test points, the points indicated with red are source points are the equilibrium test points. The welding points are classified according to the test type and are tabulated in Table 4.1.

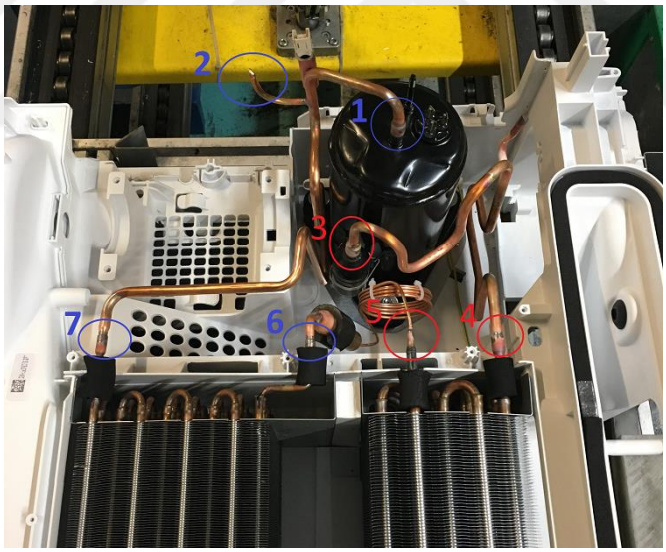

Figure 4.3 : The welding points of gas leakage test.

Table 4.1 : Classification of source points according to test type.

Type of Tests	Welding Points
High Pressure	1., 2., 6. and 7. point
Equilibrium	3., 4. and 5. point

The first test is a gas leak test that is called the high-pressure test is applied to the welding points of copper pipe which provides gas passage to the condenser after compressor operator. In this test, when the compressor is working, the pressure between 15-20 bar is formed in the copper pipes which provide the gas passage to the condenser. At this time, 3 bar pressures is formed in the copper pipes leading to the evacuation. This test is performed before the test station. The compressor is started before arriving at the test station. When the product arrives at the test station, the compressor is stopped and the high pressure test is carried out at 4 points on the copper pipe providing the condenser inlet and outlet connections.

The second test is the gas leak test that is called the equilibrium test is applied to the welding points of copper pipe which provides the gas passage of the evaporator after 10 seconds of the compressor stop. In this test, test starts after 15 seconds of stopping the compressor operator. After the compressor stops at the test station, the equilibrium test begins after the high pressure test. At this time, 3 bar pressure on the copper pipe, which supplies evaporator connections when the compressor is running, comes out of 9 bar pressure due to pressure from the condenser. Thus, the equilibrium test is carried out at 3 points on the copper pipe providing the evaporator inlet and outlet connections. As a result, a total of 7 gas leakage tests are performed at the welding points.

4.3 Vision Based Positioning

The test station, which is shown in Figure 4.4, consists of 3 components. These are ABB IRB 140 robot, camera and PLC. The communication system between these components is described in Section 2.4. The gas leak test is carried out HLD6000 Refrigerant Leak Detector is shown in Figure 2.3 on the tip of the robot. In each test cycle, the image taken from the camera at each test cycle is sent to the robotic new test positions after the image processing algorithm and the test points are determined.

Figure 4.4 : The gas leakage test station.

Thus, vision based positioning have been presented to improve the accuracy and flexibility of robotic systems is used in this thesis for gas leak test automation. The purpose of vision based positioning method is to control robot using the position information which is obtained by image processing or vision systems [52]. Vision systems are usually categorized depending on the number cameras number and their positions.

The first one is multi-camera vision systems by using two cameras in a stereo configuration make easier numerous computer vision difficulties. The second one is single camera vision systems are usually used because they are cheaper and easier to build than multi camera vision systems [53]. In this thesis, single camera vision system is used to vision based positioning of ABB IRB 140 robot for gas leak test automation.

The classification by camera position, if the camera is mounted to the robot which is called as “in-hand” systems. On the other hand, if the camera perceives the robot from which is called as “out-hand” systems [54]. In this thesis, “out-hand” system is used to vision based positioning of ABB IRB 140 robot for gas leak test automation.

The design of control scheme of vision based positioning of ABB IRB 140 robot for gas leak test automation is selected “direct visual servoing is that the vision based controller directly compute the input of the dynamic systems. [55]. The flowchart of vision based positioning of gas leak test automation can be seen in Figure 4.5.” is that the vision based controller directly compute the input of the dynamic systems.

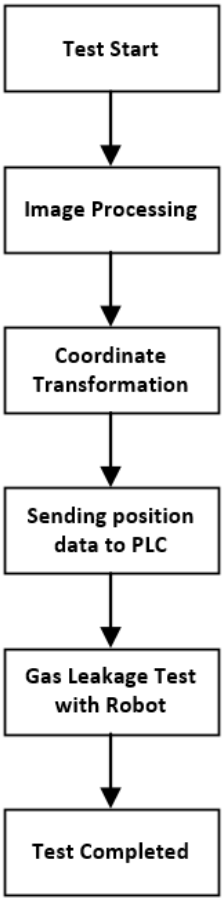

Figure 4.5 : The flowchart of test station

The test starts with the chassis arriving at the test station. When the product arrives, the information is collected from the sensor reflected from the object in the test station. After the product arrives, the camera takes the picture of the chassis and the image processing algorithm works. After the welding points are found by using image processing algorithm, the coordinate transformation of between the robot and the camera is performed. The position data of welding points in the image coordinate system is converted into the world coordinate system, which is the robot coordinate system, by using camera calibration. The position information is transferred from the PC module of the camera to the PLC via Profinet communication, and the same communication via the PLC is sent to the robot. The robot goes to the updated position information and the gas detector makes the measurement for gas leakage. If there is a leak, the gas detector sends a signal to PLC and the system alarms. After the test is completed, the test completed signal is sent from the robot to the PLC The chassis leaves the test station and continues the production line. The image processing steps, algorithms and filters are presented later in the Section 4.4.

4.4 Image Processing Algorithm for Welding Points of Gas Leakage Test

In the chassis of HP compressor, the positions of the welding points on the two pipes connected to the evaporator and the condenser from the compressor are model-based according to the depth of the product, the position shift of the chassis on the pallet and the displacement due to welding operator. In this section, the image processing algorithm defined for identifying the source points and finding the positions will be explained.

The algorithm consists of the three main stages [56]:

- research to find and select toolkits to solve the assignment
- expert handling, analysis and evaluation of image processing results interactively with the participation of NI (National Instruments) Vision Assistant tools
- automatic process with constant calculation procedures, finding the right process results.

The total chassis area is divided into 3 while the image processing algorithms according to the distance in the Z direction to camera for 7 source points in total are created. The divided areas marked with turquois are shown in the Figure 4.6.

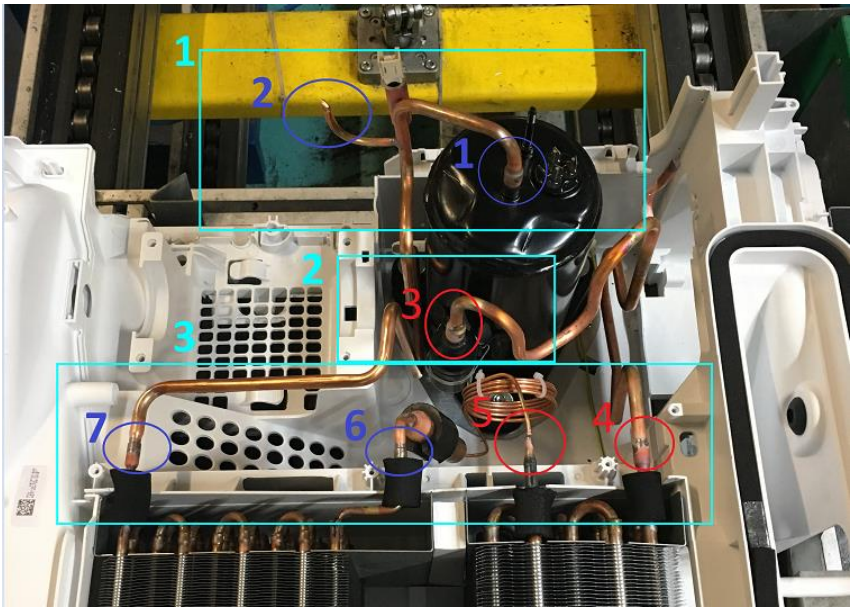

Figure 4.6 : The divided areas for image processing algorithms.

The algorithms have been created for each area separately. In these areas, the first and second welding points for the high pressure test in the first area, the third source

point for the equilibrium test in the second area, and the fourth and fifth welding points for the equilibrium test and sixth and seventh welding points for the high pressure test in the third area are found. Image processing methods which are threshold, morphological operators and color plane extractions described in Section 3.1, Section 3.2 and Section 3.3, respectively, are used in algorithms. Apart from these methods, methods such as masking and clamp are also used. The parameters have been selected for the best results in NI Vision Assistant. The complete Labview block diagram is shown in Figure 4.7. The 'True' conditions are used to operate for image processing algorithms. The image processing algorithms run in sequence, notification is generated at the end of each algorithm. The position data is transformed from image coordinate system to world coordinate system in Labview block diagram.

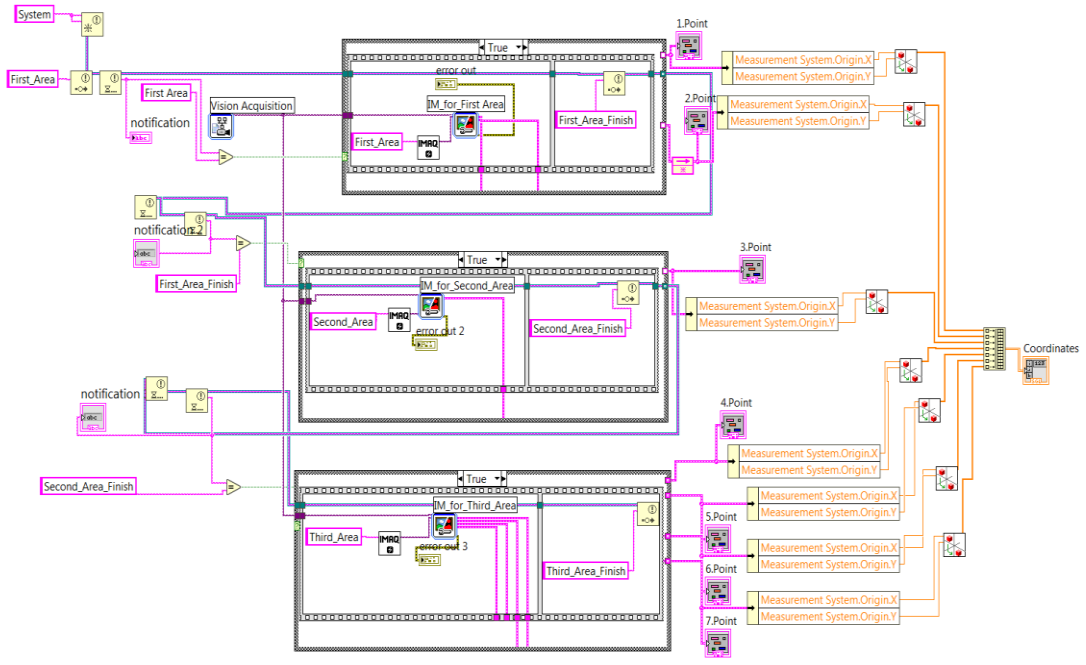

Figure 4.7: The labview block diagram.

4.4.1 Image processing algorithm for first area

The first operator is the image mask operator is used to focus processing on first area in the original image and operators to be applied to the first are limited to the restrictor rectangle. The color plane extraction is used to simplify processing by the next tools and operators. In second operator, original images can be in a RGB is converted to color image Hue Saturation Luminance (HSL) format. HSL format corresponds exactly to the grayscale image and furthermore, it is the only color plane

that will give an accurate representation of the grayscale image. The image mask and color plane extraction operators are shown in Figure 4.8 for first area.

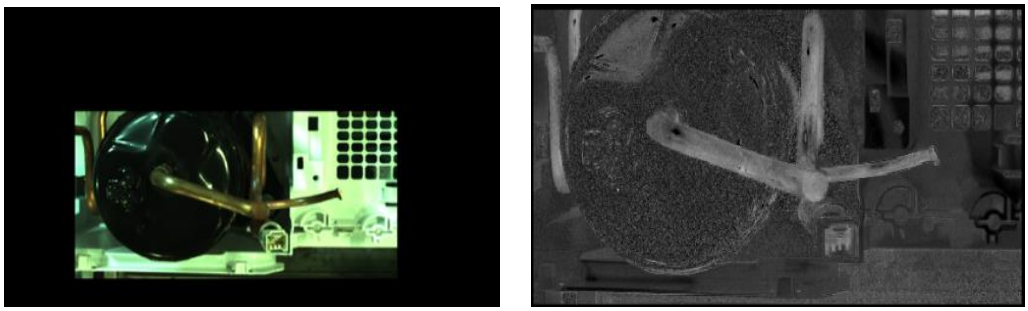

Figure 4.8 : The image mask and color plane extraction operators for first area.

The grayscale morphological operator is used to improve the quality of extraction copper pipe and to filter the pixel intensities of image. The erode operator is applied with the parameters are structuring element cross 5x5 and the number of iteration is 1. The threshold operator is used for looking for bright objects. Manual threshold method is selected with lower threshold value is selected as 73 to select pixels that are equal to or greater than the lower threshold. The grayscale morphological and threshold operators are shown in Figure 4.9 for first area.

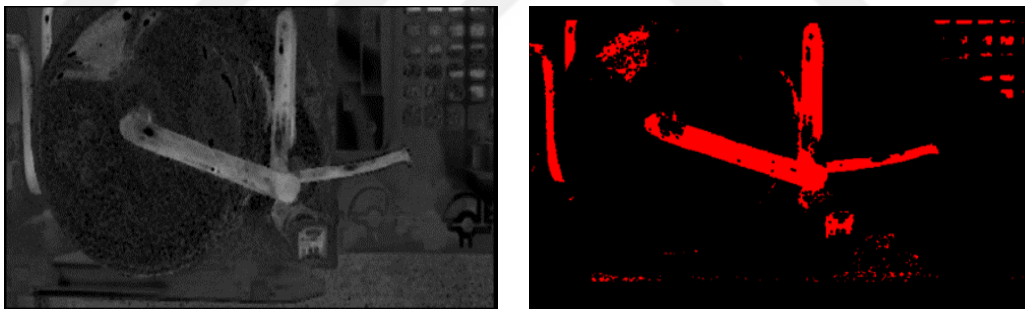

Figure 4.9 : The grayscale morphological and threshold operators for first area.

The dilate operator of basic morphological operator performs to increase the brightness of each pixel that is surrounded by neighbors with a higher intensity. The parameters of dilate operator are structuring element 3x3 and the number of iteration is selected as 2. Then, advance morphology is applied for eliminating small particles in binary image. The remove small objects operator of advance morphological performs and the iteration number of operator is 9. The first dilate and remove small objects operators are shown in Figure 4.10 for first area.

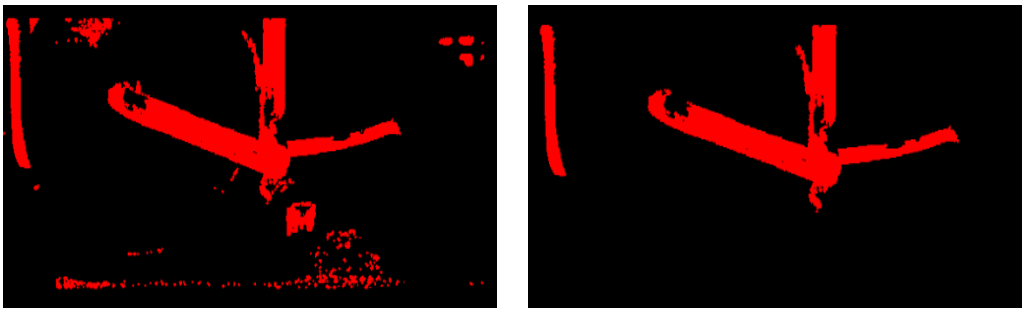

Figure 4.10 : The first dilate and remove small objects operators for first area.

The dilate operator and remove small object operators have been applied once again with larger parameters to eliminate even larger particles. The parameters of dilate operator are structuring element 5x5 and the number of iteration is 3. The iteration number of operator of remove small object operator is 25. Two operators are applied to the elimination of the pipes around the pipe where the welding points at the end points are located. The second dilate and remove small objects operators are shown in Figure 4.11 for first area.

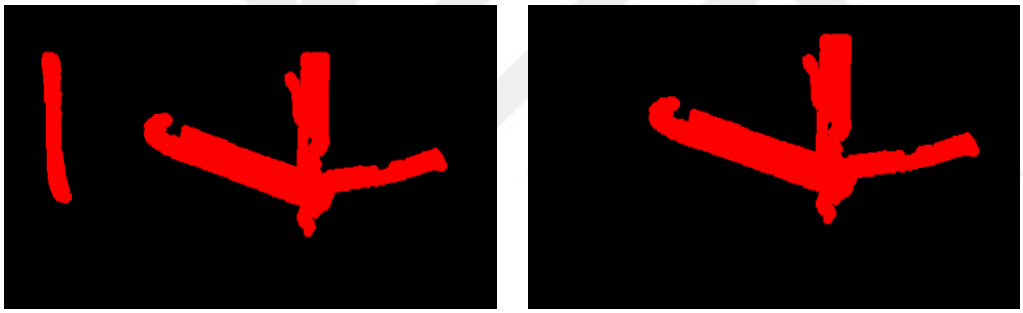

Figure 4.11 : The second dilate and remove small objects operators for first area.

The LookUp Table (LUT) operator is applied to predefined LUT transformations to the image to modify the dynamic intensity of areas in the image with poor contrast. Then, the image is applied LUT operator overlaps the image after color plane extraction in Figure 4.9. The last operator of first are is max clamp operator which finds edges within a rectangular area of interest (ROI) drawn in the image and measures the distance between the first and last edge. In this stage, the search direction of clamp operator is horizontal and angle range is selected 10 degrees. The parameters of max clamp operators are that edge threshold is selected as 50, minimum length is selected as 25, search step size is selected as 10. the edge polarity is initially determined from dark to the bright, and from the bright to the black at the end. The start and end points of the pipe from the compressor to condenser are found by using the max clamp operator. The point on the right side is determined as the

first point and the point on the left side is as the point. Therefore, two points defined in the first area are found. The max clamp operator is shown in Figure 4.12 for first area.

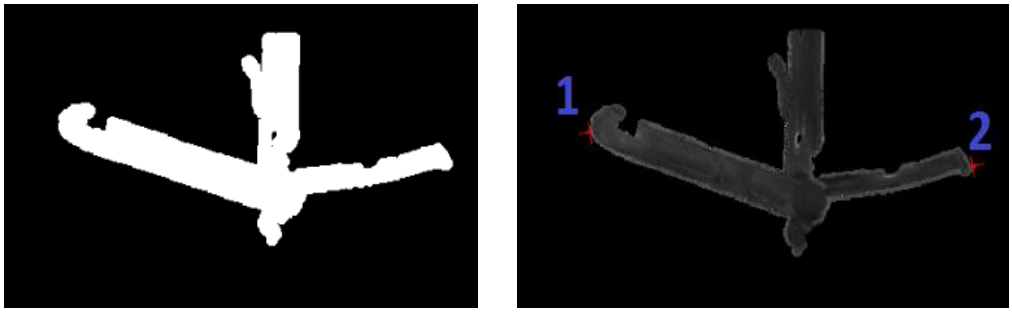

Figure 4.12 : The LUT and max clamp operator for first area.

4.4.2 Image processing algorithm for second area

The first operator is the image mask operator is used to focus processing on second area in the original image and operators to be applied to the first are limited to the restrictor rectangle. In second operator, original images can be in a RGB is converted to color image HSL format by using color plane extraction operator. HSL format corresponds exactly to the grayscale image and furthermore, it is the only color plane that will give an accurate representation of the grayscale image. The image mask and color plane extraction operators are shown in Figure 4.13 for second area.

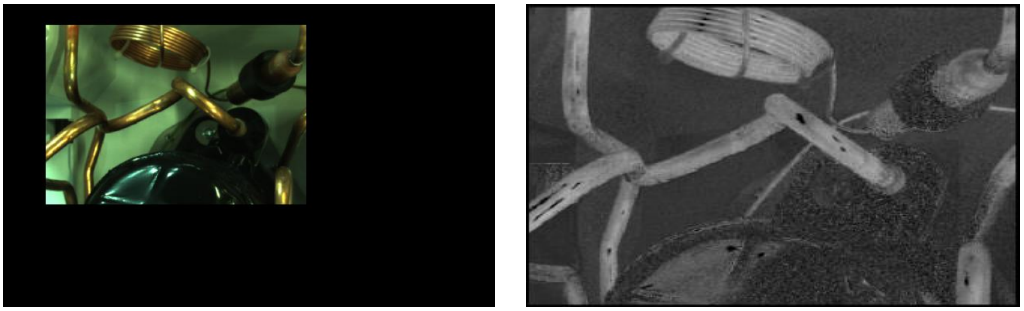

Figure 4.13 : The image mask and color plane extraction operators for second area.

The erode operator of gray morphology is applied with the parameters are structuring element cross 5x5 and the number of iteration is 1. Manual threshold of threshold operator is selected with lower threshold value is selected as 82 to select pixels that are equal to or greater than the lower threshold. The grayscale morphological and threshold operators are shown in Figure 4.14 for second area.

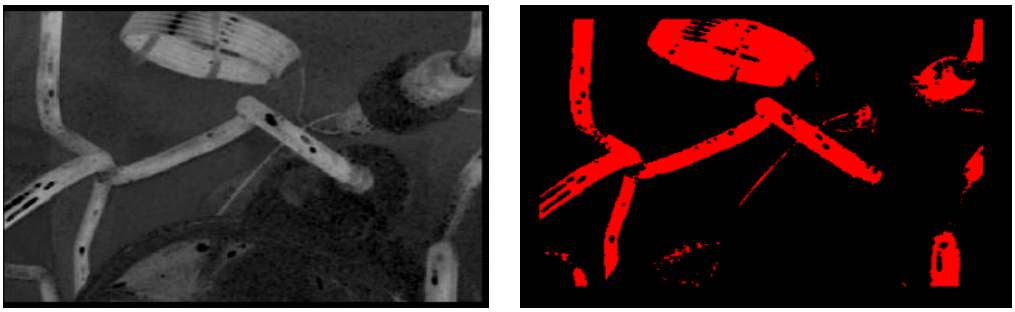

Figure 4.14 : The grayscale morphological and threshold operators for second area.

The close operator of basic morphological operator performs for small holes are removed and gaps are filled in the object boundaries. The parameters of close operator are structuring element 4x4 and the number of iteration is selected as 1. After, advance morphology is applied for eliminating small particles in binary image. The remove small objects operator of advance morphological performs and the iteration number of operator is 11. The close and remove small objects operators are shown in Figure 4.15 for second area.

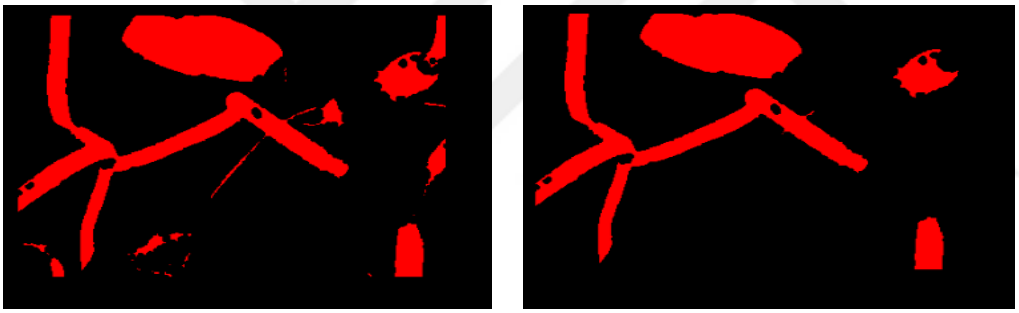

Figure 4.15 : The close and remove small objects operators for second area.

The dilate operator performs to improve the brightness of each pixel and the parameters of dilate operator are structuring element 9x9 and the number of iteration is selected as 2. The parameters have been chosen to be large because the particle filter particle filter that isolates and keeps the circular particles and removes the non-circular particles from the image. will be used as the next operator. Thus, other pipes outside the main pipe from the compressor will be eliminated. The parameters of particle filter which are minimum value is selected as 6000 and maximum value is selected as 500000. The dilate and particle filter operators are shown in Figure 4.16.

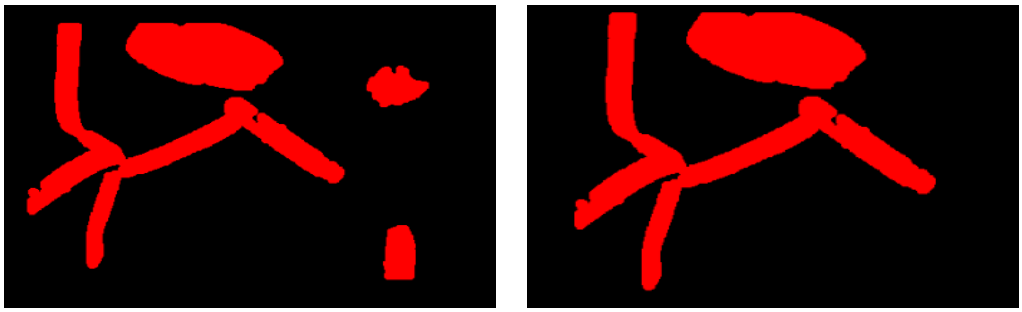

Figure 4.16 : The dilate and particle filter operators for second area.

The LUT operator is applied to image which is applied threshold and the image is applied LUT operator overlaps the image after color plane extraction in Figure 4.14. The final operator is max clamp operator is applied with the search direction of clamp operator is horizontal and angle range is selected 30 degrees. The parameters of max clamp operators are that edge threshold is selected as 70, minimum length is selected as 200, search step size is selected as 100. the edge polarity is initially determined from dark to the bright, and from the bright to the black at the end. The start point of the pipe is determined on the right side from the compressor to evaporator is found by using the max clamp operator. Therefore, third point of welding defined in the first area is found. The LUT and max clamp operators are shown in Figure 4.17 for second area.

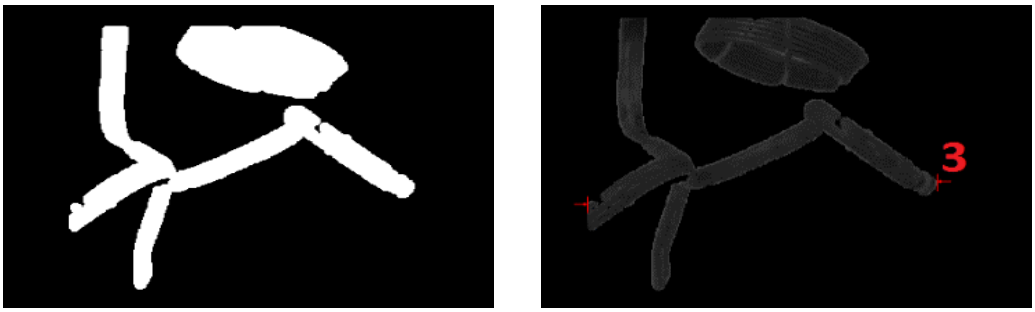

Figure 4.17 : The LUT and max clamp operators for second area .

4.4.3 Image processing algorithm for third area

The first operator is the image mask operator is used to focus processing on third area in the original image and operators to be applied to the first are limited to the restrictor rectangle. In second operator, original images can be in a RGB is converted to color image HSL format by using color plane extraction operator. The image mask and color plane extraction operators are shown in Figure 4.18 for third area.

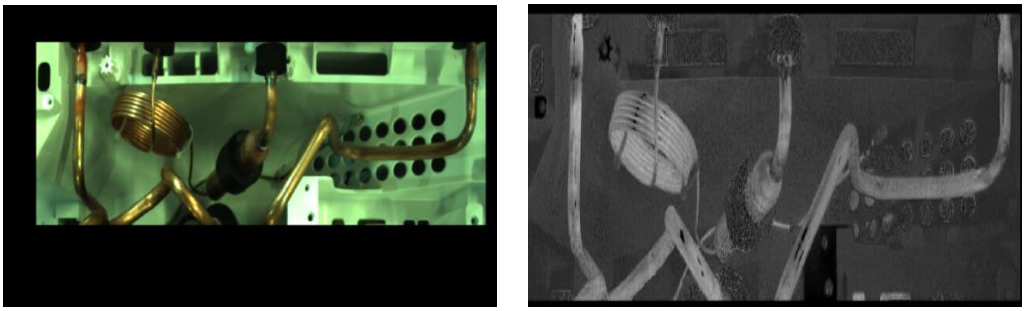

Figure 4.18 : The image mask and color plane extraction operators for third area.

The dilate operator of gray morphology is applied with the parameters are structuring element cross 3x3 and the number of iteration is 1. Manual threshold of threshold operator is selected with lower threshold value is selected as 95 to select pixels that are equal to or greater than the lower threshold. The grayscale morphological and threshold operators are shown in Figure 4.19 for third area.

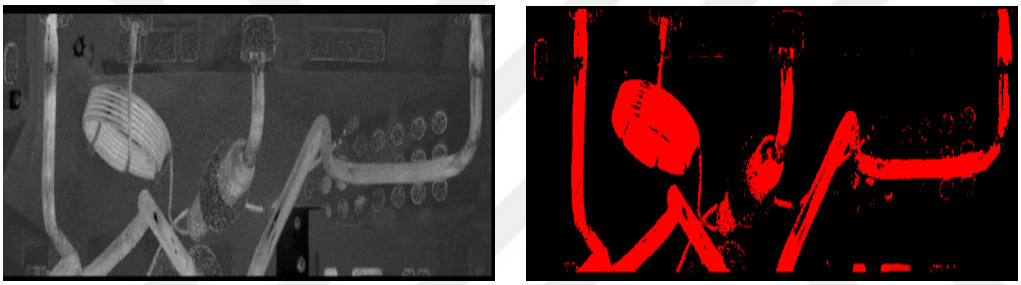

Figure 4.19 : The grayscale morphological and threshold operators for third area.

The close operator of basic morphological operator performs and The parameters of close operator are structuring element 7x7 and the number of iteration is selected as 1. After, advance morphology is applied for eliminating small particles in binary image. The remove small objects operator of advance morphological performs and the iteration number of operator is 9. The close and remove small objects operators are shown in Figure 4.20 for third area.

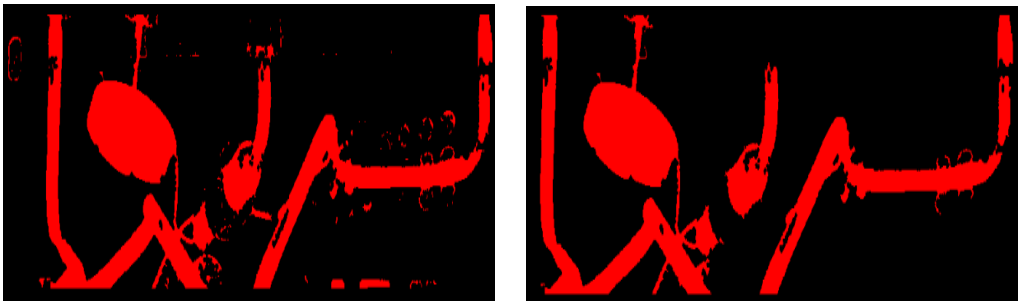

Figure 4.20 : The close and remove small objects operators for second area.

The dilate and erode operators of gray morphology are applied respectively For filling the gaps in the pipes and for the integrity of the pipes. The parameter of dilate operator are structuring element cross 9x9 and the number of iteration is 2. The parameter of erode operator are structuring element cross 5x5 and the number of iteration is 2. The gray morphological operators are shown in Figure 4.21 for third area.

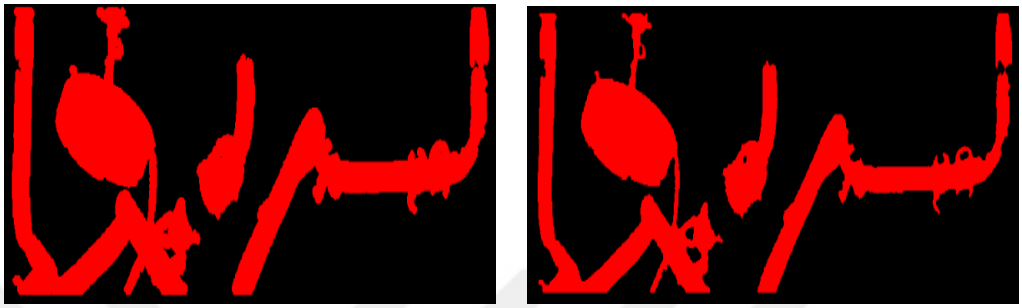

Figure 4.21 : The dilate and erode operators for third area.

The LUT operator is applied to image which is applied threshold and the image is applied LUT operator overlaps the image after color plane extraction in Figure 4.9. The final operator is max clamp operator is applied four times for four welding points with the search direction of clamp operator is vertical. The parameters of first max clamp operator are that angle range is selected 10 degrees, edge threshold is selected as 10, minimum length is selected as 25, search step size is selected as 10. The parameters of second max clamp operator are that angle range is selected 10 degrees, edge threshold is selected as 60, minimum length is selected as 100, search step size is selected as 20. The parameters of third max clamp operator are that angle range is selected 5 degrees, edge threshold is selected as 50, minimum length is selected as 75, search step size is selected as 75. The parameters of fourth max clamp operator are that angle range is selected 10 degrees, edge threshold is selected as 40, minimum length is selected as 200, search step size is selected as 100. The edge polarity is initially determined from dark to the bright, and from the bright to the black at the end for all max clamp operators. The starts point of the pipe is determined on the upside from the compressor to condenser for the fourth and fifth welding points and from the compressor to evaporator the sixth and seventh source points are found by using the max clamp operator.

Therefore,last four points of welding defined in the first area is found. The LUT and max clamp operators are shown in Figure 4.22 for third area.

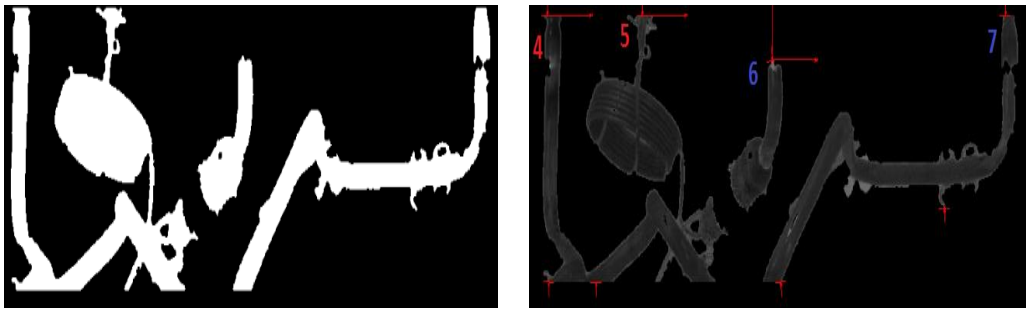

Figure 4.22 : The LUT and max clamp operators for second area.

5. EXPERIMENTAL RESULTS

In this section, the results of vision based positioning of ABB IRB 140 robot test automation for gas leakage control are presented. The real-time studies are carried out for the vision based positioning for seven welding points of the high pressure and equilibrium test and configurations using Vision Assistant Express in Labview and RobotStudio. The position information of the welding points is collected from for 500 products. In this study, a camera is mounted from the top is used in the test station. As a result of the real time studies the deviation of position coordinates of the X and Y axis are shown and interpreted in the world coordination system for seven welding points for the high pressure and equilibrium test. Finally, the mean, standard deviation, quartile, minimum and maximum values of deviations are presented on X and Y axis for the high pressure and equilibrium tests.

5.1 Updating The Camera Calibration Parameters

The camera is calibrated using the procedure described in the Section 3.4. The position in Z direction (depth) of the welding points are fixed for each welding points. In this direction, the camera calibration to develop a mathematical model of the transformation between world points and observed image points resulting from the image formation process is done third times according to the image processing areas of welding points. The camera calibration is made to a depth of 220 cm in the equation (3.23).

The distances from the camera in the Z direction are selected as 275 cm for the first area, selected as 300 cm for the second area and selected as 325 cm for the third area. The parameters have been updated according to the new depth value and camera calibration is used. The updated parameters for each area are given in Table 5.1 according to the equation (3.22).

Table 5.1 : Camera calibration parameters.

Area	A	B	C	D	E	F
1	3.85	2.47	98.66	0.95	0.64	25.36
2	4.17	2.63	102.34	1.22	0.78	29.74
3	4.49	2.84	116.72	1.64	1.05	39.47

5.2 High Pressure Test Results

In this subsection, the deviation of the welding points in the tested products for the high pressure test with the vision based positioning in the test station is examined according to the robot position data. The welding points are tested on the high pressure test are given in Table 4.1.

The deviation between first welding point positions for 500 sample products on the X and Y axis of first welding points are illustrated in Figure 5.1 and Figure 5.2. As can be seen from the figures, there is no effect of operator induced changes on the X axis for the first point because there is no displacement in the welding at the outlet of the compressor. However, due to the displacement of the compressor on the product, a displacement of about 100 mm is observed. On the Y axis, ±30 mm displacement is constantly visible the compressor can be interpreted as a position change on the frame on the Y axis.

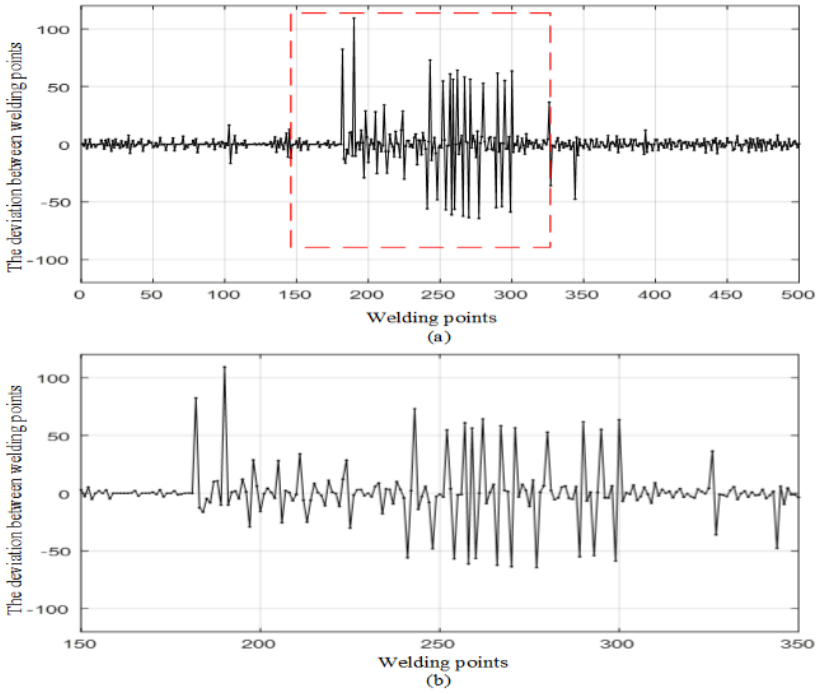

Figure 5.1 : The deviation (a) all (b) peak first welding points on X axis.

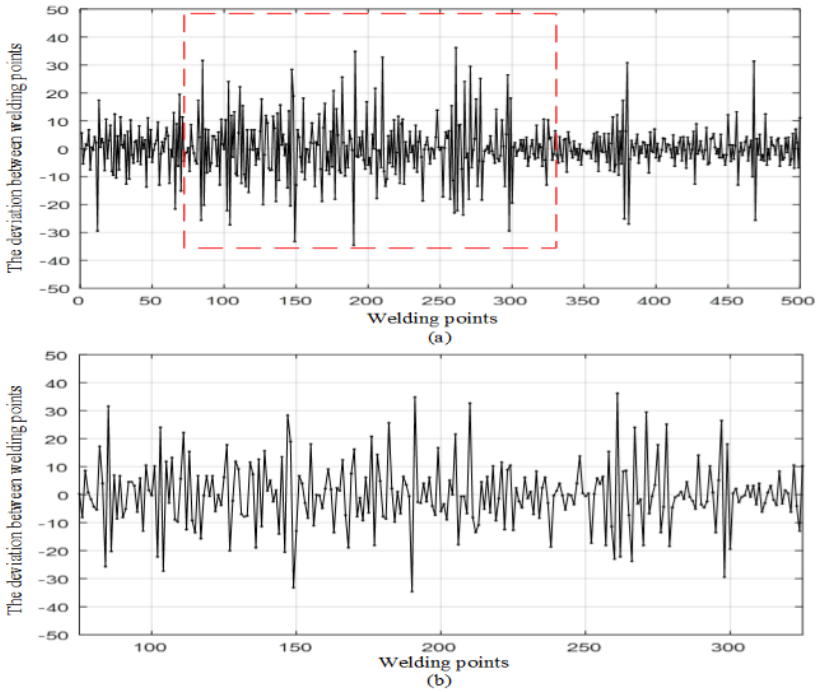

Figure 5.2 : The deviation (a) all (b) peak first welding points on Y axis.

The deviation between second welding point positions for 500 sample products on the X and Y axis of second welding points are illustrated in Figure 5.3 and Figure 5.4. As can be seen from the figures, the deviation in positional changes in the X and Y axis at the second source point is more frequent. It is shown that the change in the end point of the pipe does not result from the effect of the model change, but rather the position changes due to the operator influence during the welding operator.

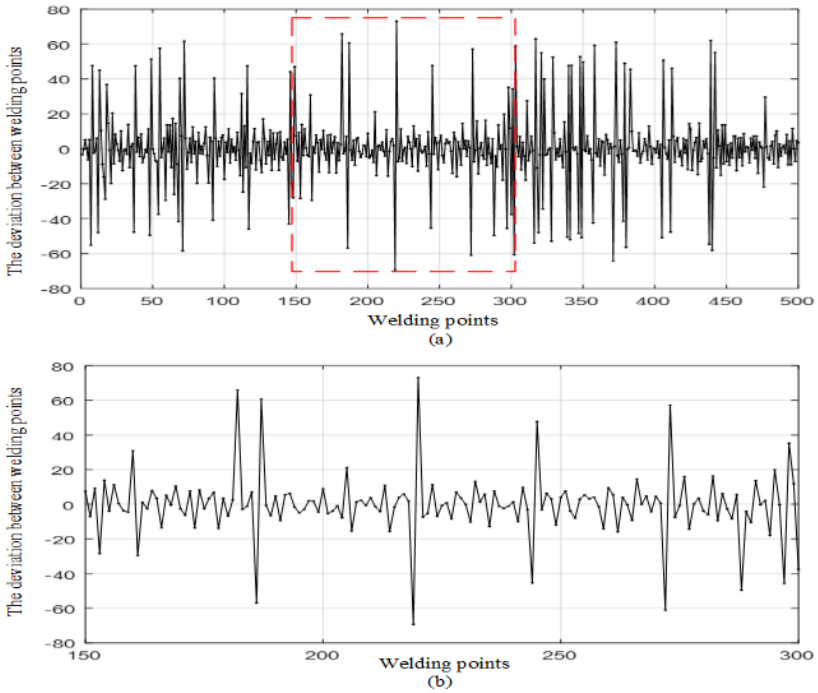

Figure 5.3 : The deviation (a) all (b) peak second welding points on X axis.

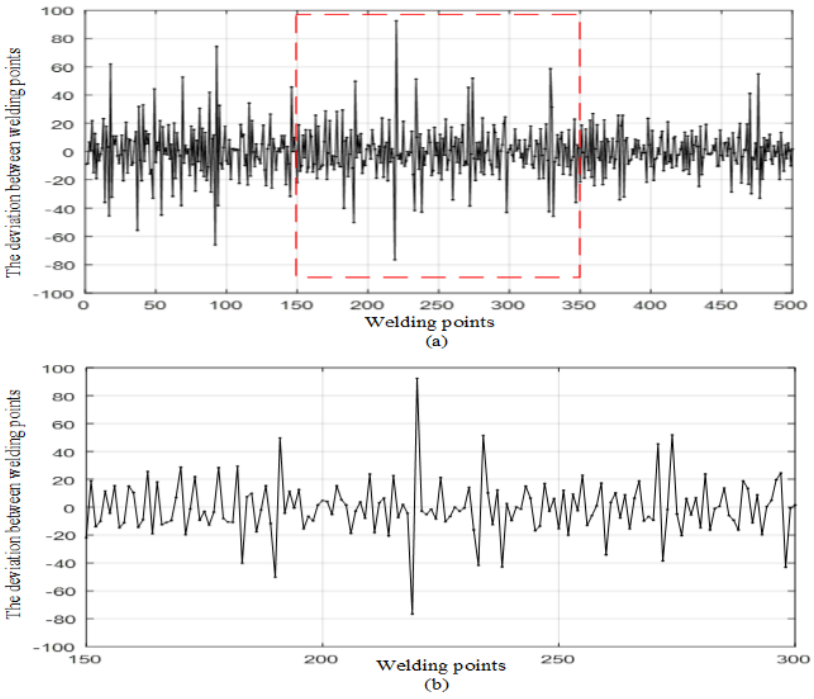

Figure 5.4 : The deviation (a) all (b) peak second welding points on Y axis.

The deviation between sixth welding point positions for 500 sample products on the X and Y axis of sixth welding points are illustrated in Figure 5.5 and Figure 5.6. As can be seen from the figures, the deviations are a wide range due to model transitions, as the deviations at the sixth welding point at the compressor inlet similar at the fifth welding point. In various models, the compressors are used in different

sizes. Since the compressor is not referenced to a certain point when it is placed in the product, the positions deviate in the X direction at the sixth source point. The deviations on the Y axis are occurred in the narrow range due to the deviations the position of the product on the palette to the palette dimensions.

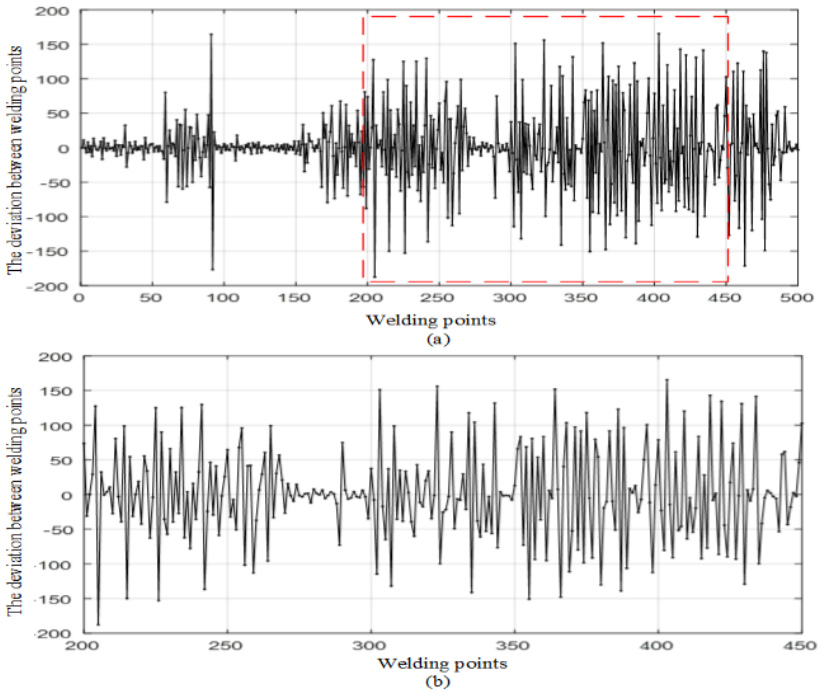

Figure 5.5 : The deviation (a) all (b) peak sixth welding points on X axis.

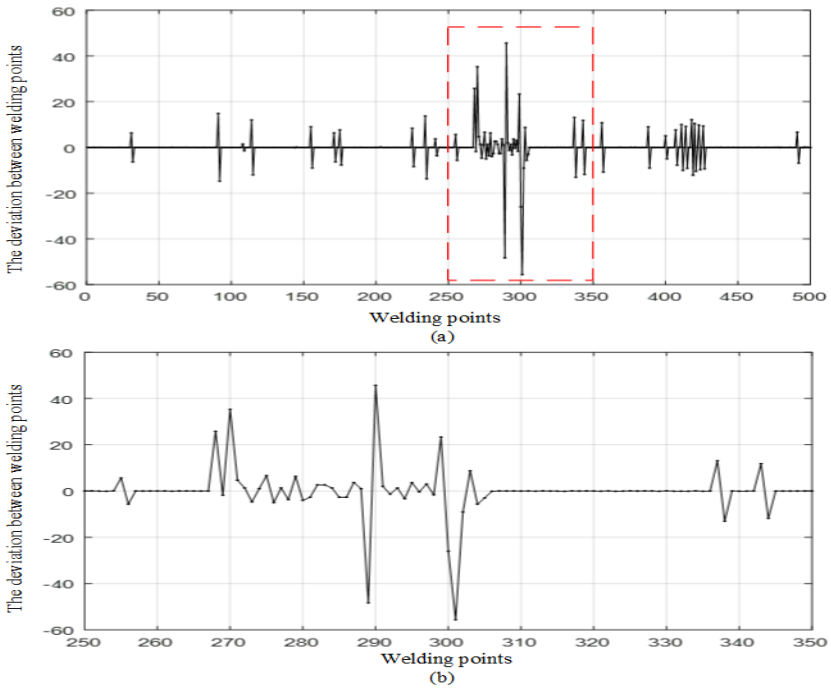

Figure 5.6 : The deviation (a) all (b) peak sixth welding points on Y axis.

The deviation between seventh welding point positions for 500 sample products on the X and Y axis of seventh welding points are illustrated in Figure 5.7 and Figure 5.8. As can be seen from the figures, like the sixth welding point, the deviations at the seventh welding point at the compressor outlet are a wide range due to model transitions. The compressors are used in different sizes. Since the compressor is not referenced to a certain point when it is placed in the product, the positions deviate in the X direction at the seventh source point. The deviations on the Y axis are occurred in the narrow range due to the deviations the position of the product on the palette to the palette dimensions.

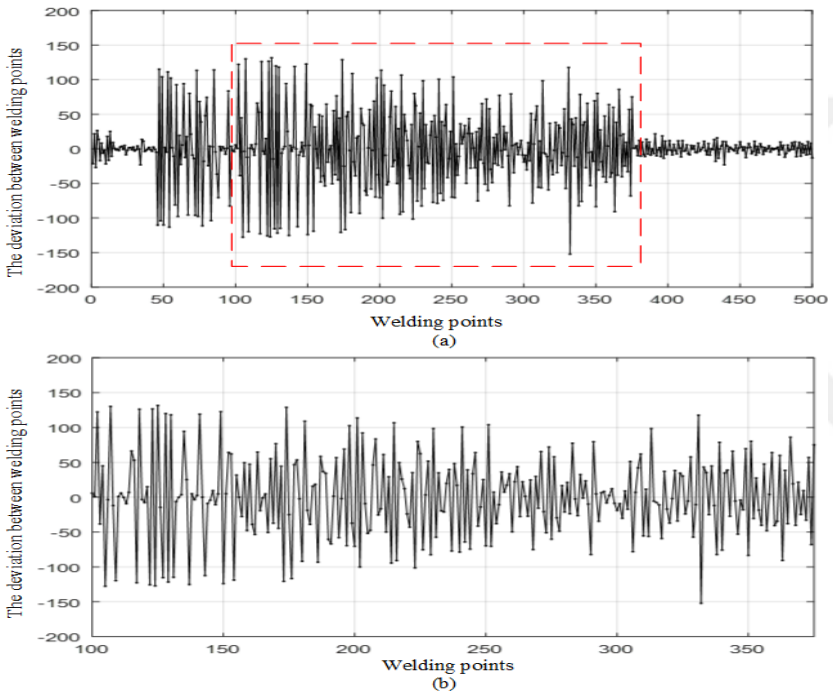

Figure 5.7 : The deviation (a) all (b) peak seventh welding points on X axis.

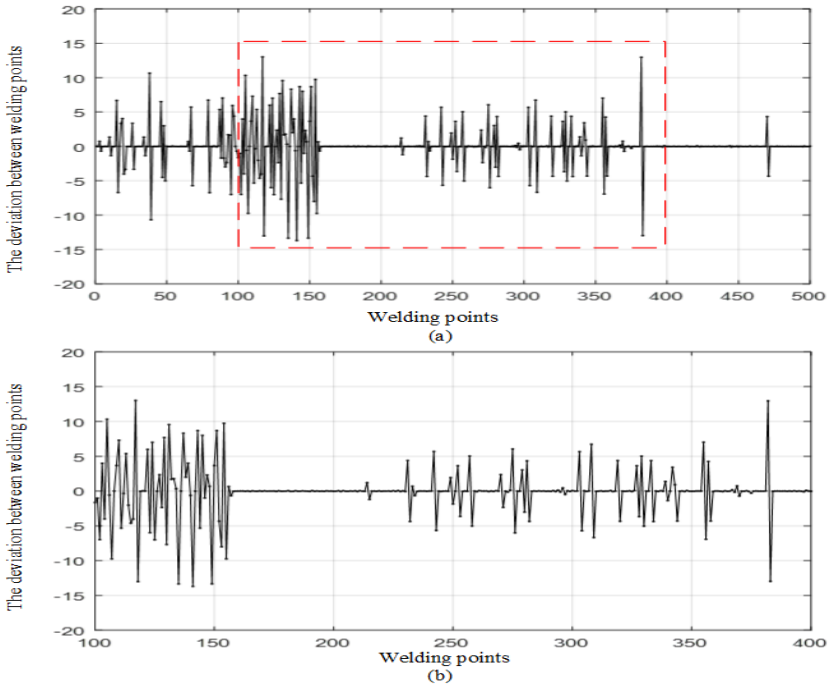

Figure 5.8 : The deviation (a) all (b) peak seventh welding points on Y axis.

Firstly, the mean, standard deviation, 1st quartile and 3rd quartile of the deviations, minimum and maximum values on the X axis for the high pressure test are given in Table 5.2.

Table 5.2 : The descriptive statictics of deviations on the X axis for high pressure.

Welding Points	Mean	Standard Deviation	1st Quartile	3nd Quartile	Minimum	Maximum
1	0.005	16.02	-2.65	2.36	-64.30	109.30
2	0.007	20.92	-6.82	6.28	-69.23	73.11
6	0.110	56.07	-17.25	16.94	-187.80	165.50
7	-0.110	49.91	-17.18	17.18	-152.30	131.80

As a result of the descriptive statistics of position data in Table 5.1, the mean values of the welding points is close to 0. It can be said that the welding points are around certain points, but it is not possible to interpret the deviation effect by using the mean value. In standard deviations, the standard deviations are higher at the welding points that are sixth and seventh the welding points for the high pressure test where the position change is due to the model difference on the X axis. In the same way the quartile interval is higher. On the other hand, it is seen that the standard deviation value and quartile interval at the first and second welding points for the high pressure test are lower. It has been observed that the deviation value at these points is operator sourced during the welding operator. At these points, it has been shown that the

vision based positioning application for ABB IRB 140 robot is required for gas leakage test. If conventional robot programming without vision based positioning had been applied, the welding points for the gas leak test at these points would be missed and the automatic test with ABB IRB 140 robot would be failed.

Secondly, the mean, standard deviation, 1st quartile and 3rd quartile of the deviations, minimum and maximum values on the Y axis for the high pressure test are given in Table 5.3.

Table 5.3 : The descriptive statictics of deviations on the Y axis for high pressure.

Welding Points	Mean	Standard Deviation	1st Quartile	3nd Quartile	Minimum	Maximum
1	-0.007	9.86	-4.806	4.595	-34.58	36.23
2	0.120	18.24	-9.664	9.484	-76.49	92.43
6	-0.001	5.56	-0.028	0.026	-55.65	45.66
7	-0.001	2.97	-0.032	0.030	-13.70	12.96

As a result of the descriptive statictics of position data in Table 5.3, the mean values of all the welding points is close to 0 on the Y axis as in the deviations on the X axis. It can be said that the all welding points on the Y axis are around a certain point. In standard deviations, that the standard deviations on the Y axis are less than the standard deviations on the X axis. In particular, deviations due to model differences on the X axis are very small on the Y axis. For this reason, it can be said that the deviations on the Y axis are caused by the size variation of the position of product on the pallet and the dimension of pallets rather than the model change. The variation is over the quartile intervals at the observed the welding points. At these points, it has been shown that the vision based positioning application for ABB IRB 140 robot is required for gas leakage test. If conventional robot programming without vision based positioning had been applied, the welding points for the gas leak test at these points would be missed and the automatic test with ABB IRB 140 robot would be failed.

5.3 Equilibrium Test Results

In this subsection, the deviation of the welding points in the tested products for the equilibrium test with the vision based positioning in the test station is examined according to the robot position data. The welding points are tested on the equilibrium test are given in Table 4.1.

The deviation between third welding point positions for 500 sample products on the X and Y axis of third welding points are illustrated in Figure 5.9 and Figure 5.10. As can be seen from the figures, the position deviations on the X and Y axis initially are few. However, after 300 deviations, the deviations of welding positions are more visible in the X and Y directions. As the welding operator is carried out on the pipe above the compressor, the deviations appear to be due to the positional change of the compressor in the chassis and the position deviation of the chassis on the pallet.

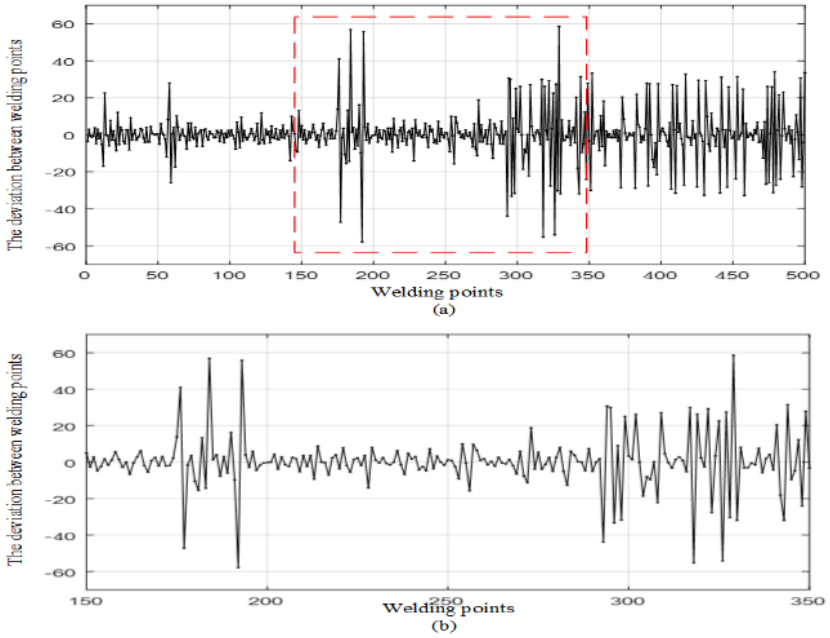

Figure 5.9 : The deviation (a) all (b) peak third welding points on X axis.

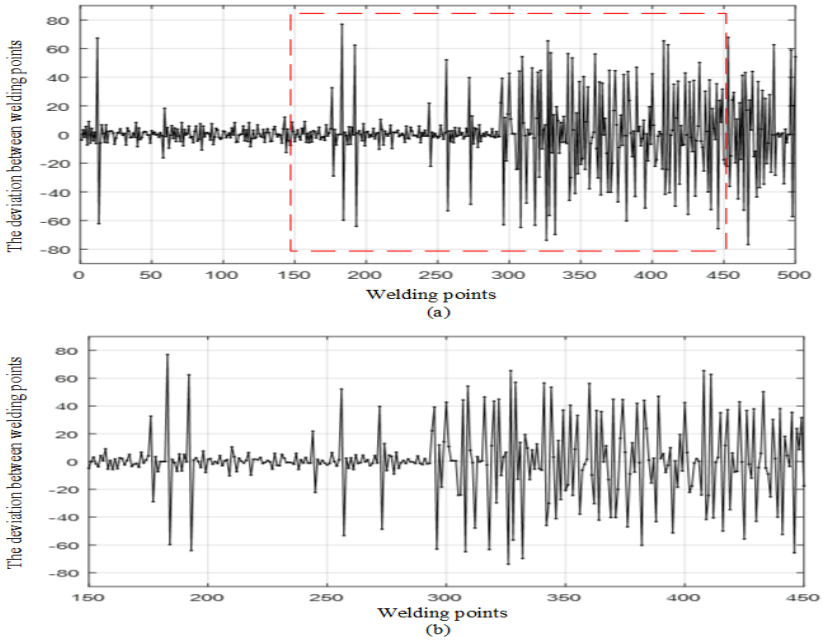

Figure 5.10 : The deviation (a) all (b) peak third welding points on Y axis.

The deviation between fourth welding point positions for 500 sample products on the X and Y axis of fourth welding points are illustrated in Figure 5.11 and Figure 5.12. As can be seen from the figures, the deviation in positional changes of fourth welding point which is located at the entrance of evaoperator is occurred narrow gap on the X and Y axis. There does not appear to be a change of place among the models at this welding point. However, because of the chasis playing on the pallet and due to the dimensional differences in the pallets, the deviations occur on the X and Y axis.

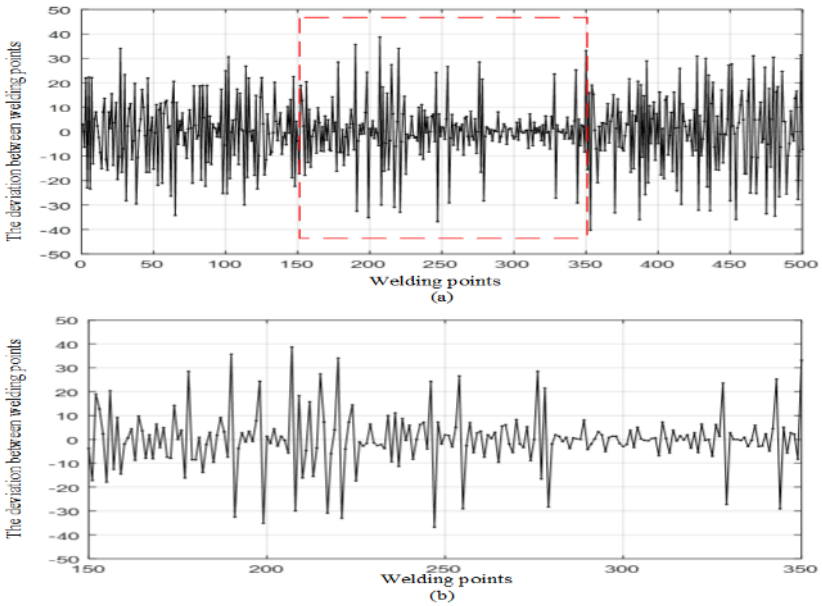

Figure 5.**11 :** The deviation (a) all (b) peak fourth welding points on X axis.

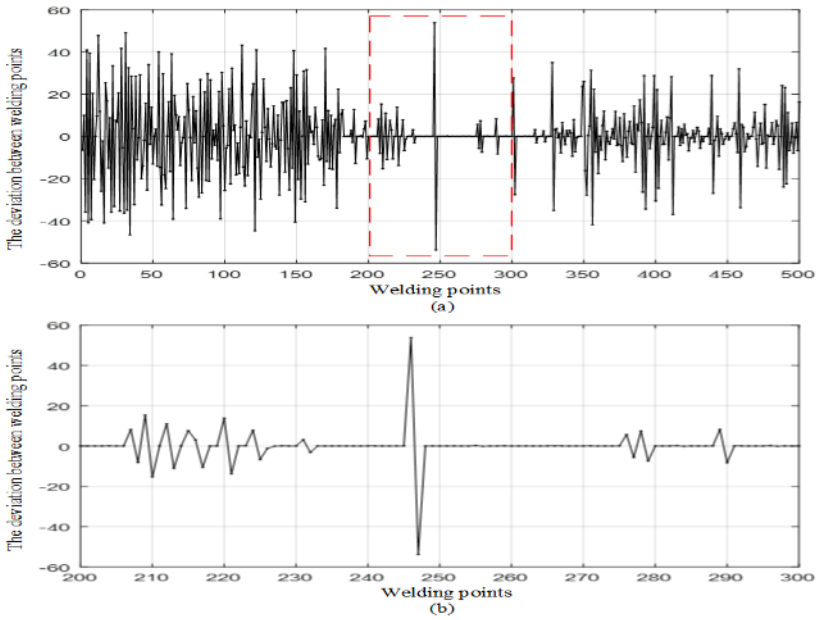

Figure 5.**12 :** The deviation (a) all (b) peak fourth welding points on Y axis.

The deviation between fifth welding point positions for 500 sample products on the X and Y axis of third welding points are illustrated in Figure 5.13 and Figure 5.14. As can be seen from the figures the deviations on X axis at the fifth welding point which is located the exit of the evaoperator are in wide range because of model transitions. The evaoperatos are used in different size in various models. As th eevaoperatos are referenced to the left while being placed on the product, the deviations in the fifth welding point are occured in X direction. The deviations on the Y axis are occurred in the narrow range due to the deviations the position of the product on the palette to the palette dimensions.

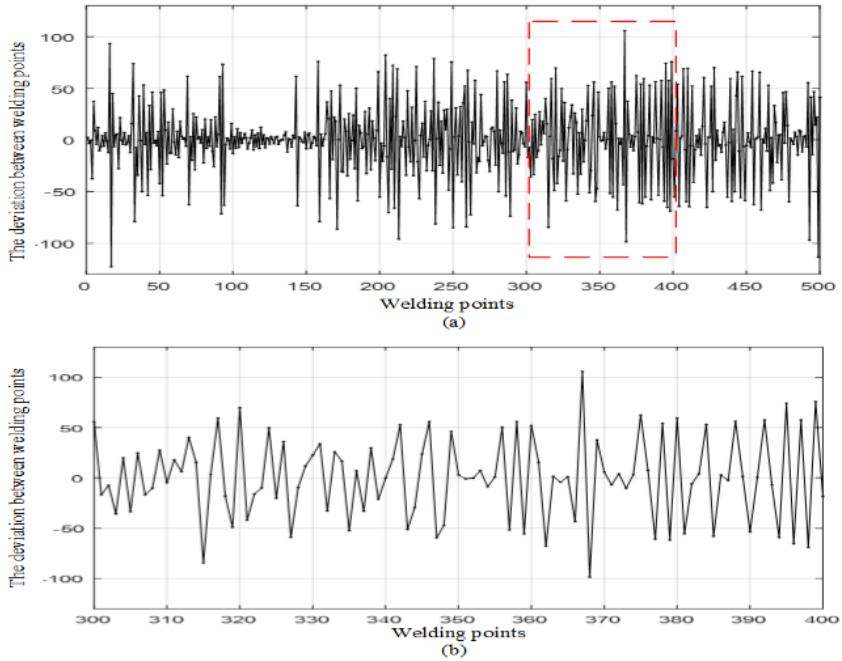

Figure 5.13 : The deviation (a) all (b) peak fifth welding points on X axis.

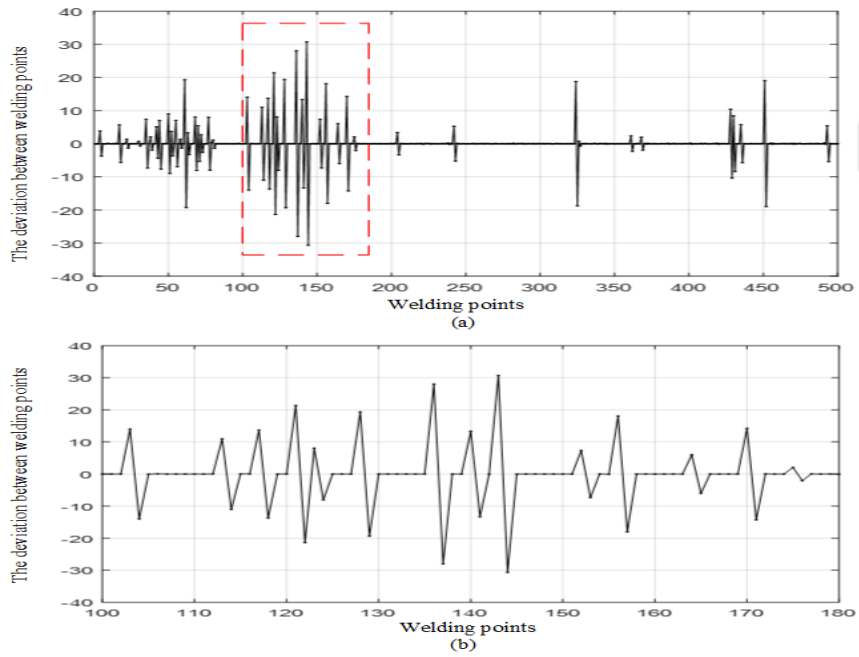

Figure 5.14 : The deviation (a) all (b) peak fifth welding points on Y axis.

Firstly, the mean, standard deviation, 1st quartile and 3rd quartile of the deviations, minimum and maximum values on the X axis for the equilibrium test are given in Table 5.4.

Table 5.4 : The descriptive statictics of deviations on the X axis for equilibrium.

Welding Points	Mean	Standard Deviation	1st Quartile	3nd Quartile	Minimum	Maximum
3	0.057	13.452	-3.60	3.28	-57.86	58.59
4	0.002	14.153	-7.45	7.27	-40.39	38.70
5	0.020	35.920	-14.44	16.76	-122.80	93.26

As a result of the descriptive statistics of position data in Table 5.3, the mean values of the welding points for equilibrium tests are close to 0 like as the welding points for high pressure test. It can be said that the welding points are around certain points, but it is not possible to interpret the deviation effect by using the mean value. In standard deviations, the standard deviations are higher at the welding points that are fifth the welding points for the equilibrium test where the position change is due to the model difference on the X axis. In the same way the quartile interval is higher. On the other hand, it is seen that the standard deviation value and quartile interval at the third and fourth welding points for the equilibrium test are lower. It has been observed that the deviation value at these points is operator sourced during the welding operator. At these points, it has been shown that the vision based positioning application for ABB IRB 140 robot is required for gas leakage test. If conventional robot programming without vision based positioning had been applied, the welding points for the gas leak test at these points would be missed and the automatic test with ABB IRB 140 robot would be failed.

Secondly, the mean, standard deviation, 1st quartile and 3rd quartile of the deviations, minimum and maximum values on the Y axis for the equilibrium test are given in Table 5.5.

Table 5.**5 :** The descriptive statictics of deviations on the Y axis for equilibrium.

Welding Points	Mean	Standard Deviation	1st Quartile	3nd Quartile	Minimum	Maximum
3	0.160	22.610	-5.34	4.80	-76.76	77.03
4	0.043	15.910	-4.36	5.70	-53.75	53.77
5	0.000	4.821	-0.03	0.03	-30.64	30.71

As a result of the descriptive statistics of position data in Table 5.5, the mean values of all the welding points for the equilibrium test is close to 0 on the Y axis as in the deviations on the X axis. It can be said that the all welding points on the Y axis are around a certain point. In standard deviations, that the standard deviations on the Y axis are less than the standard deviations on the X axis. In particular, deviations due

to model differences on the X axis are very small on the Y axis. For this reason, it can be said that the deviations on the Y axis are caused by the size variation of the position of product on the pallet and the dimension of pallets rather than the model change. The variation is over the quartile intervals at the observed the welding points. At these points, it has been shown that the vision based positioning application for ABB IRB 140 robot is required for gas leakage test. If conventional robot programming without vision based positioning had been applied, the welding points for the gas leak test at these points would be missed and the automatic test with ABB IRB 140 robot would be failed.

6. CONCLUSION

In this Master thesis, the automation project with vision based positioning by using ABB IRB 140 robot is proposed, the coordinate transformation and camera calibration is applied, two types gas leakage test for HP dryers are proposed and the image processing algorithms for welding points of gas leakage test by dividing three areas of chassis are proposed. For this purpose, the robotic automation system has been installed and the real-time experimental studies are performed in order to show the effectiveness of the vision based positioning ABB IRB 140 robot for the gas leakage test by presentation the derivations of welding points positions.

Firstly, the automatic test station consists of Siemens S1200 PLC, ABB IRB 140 robot and camera with controlling PC module is set up for the gas leakage test on the production line. ABB IRB 140 robot and camera in the test station are communicated to PLC by using Profinet communication protocol. The signals which are used between the robot and the PLC are that the current position values by obtaining camera calibration from PLC to ABB IRB 140 robot and the information of test completed knowledge from ABB IRB 140 robot to PLC. Moreover, the signals which are used between the camera with control module and the PLC are that the information of new product arrived and image processing starting from PLC to camera and the current position values and transformation values from camera to PLC. The process of the test station is formed as starting with the product arrived signal. Then, the camera takes picture and the image processing algorithms are performed and the position of welding points are determined. The coordinate values of the welding points are transformed from the image coordinate system to the world coordinate system of ABB IRB 140 robot. ABB IRB 140 is performed the gas leakage test according to the current positions value. Finally, ABB IRB 140 robot sends test finished signal and the product leaves test station.

Secondly, the image processing algorithms have been established to determine the welding points of copper pipes by using NI Vision Assistant. The whole test area is divided into three parts and three test algorithms are created. In three image

processing algorithms, firstly, the mask operators is used in the original image in order to limit the restrictor rectangle. The threshold operator is used to make the copper pipe become apparent in the image. The parameters of threshold operator are selected as 72,82 and 93. After the threshold method, the morphological operators have been applied more than once in the same algorithm to eliminate images with constraints values close to the copper pipe and maintain the pipes having the welding points. The parameters are determined according to the needs of the image processing algorithms. One of these operators is that the erode operators are applied these parameters are structuring element cross 5x5 and the numbers of iteration are selected 1 and 2. Then, the other operator is that the dilate operators are applied these parameters are structuring element cross 3x3, 5x5 and 9x9 and the number of iteration are selected 1. Then, the last operator is that the close operators are applied these parameters are structuring element cross 4x4 and 7x7 and the number of iteration are selected 1. After the copper pipe is obtained, The LUT operator is applied to the image to modify the dynamic intensity of areas in the image with poor contrast and the image is applied LUT operator overlaps the image after color plane extraction. Finally, the max clamp operators is applied in three image processing algorithms for finding the welding points in ROI. Therefore, seven welding points are found when three image algorithms are run in Labview consecutively.

Thirdly, two types of tests which are the high pressure and equilibrium tests have been proposed based on the copper pipes from compressor to condenser or evaporator for gas leakage. In the real time experimental studies, the position deviations at the welding points are collected after the vision based positioning ABB IRB 140 robot application. Initially, the deviations at four welding points, which are called as first, second, sixth and seventh welding points, are located on copper pipes from the compressor to the condenser have been investigated in the high pressure test. The mean, standard deviation, quartile, minimum and maximum values of the deviations at these welding points are also presented. When the results are examined, the deviations of the sixth and seventh welding points for the high pressure test due to the model difference on the X axis. Moreover, the deviations of the first and second welding points for the high pressure test due to operator sourced during the welding operator on the X axis. On the other hand, the deviations of four welding points in the high pressure test on the Y axis are caused by the size variation of the

position of product on the pallet and the dimension of pallets rather than the model change.

Furthermore, in the experimental studies, the deviations at three welding points, which are called as third, fourth, fifth welding points, are located on copper pipes from the compressor to the evaporator have been investigated in the equilibrium test. The mean, standard deviation, quartile, minimum and maximum values of the deviations at these welding points are also presented. When the results are examined, the deviations of the fifth welding points for the equilibrium test due to the model difference on the X axis. Moreover, the deviations of the third and fourth welding points for the equilibrium test due to operator sourced during the welding operator on the X axis. On the other hand, the deviations of three welding points in the equilibrium test on the Y axis are caused by the size variation of the position of product on the pallet and the dimension of pallets rather than the model change.

It can be concluded that, the deviations of the welding points in the high pressure test have been investigated. It is seen that the amount of deviations at the 6. and 7. welding points is more in the X axis and the amount of deviations at the 1. and 2. welding points is less in the X axis. In the high pressure test, there is a minimum deviations of -187.8 mm and a maximum of 165.5 mm on the X axis. For this reason, it was observed that the ABB IRB 140 robot with image-based positioning on the X-axis was successful. Also, minimum deviation of -76.49 mm and a maximum of 92.43 mm was observed on the Y-axis in the high pressure test. Then, the position deviation values of the welding points in the equilibrium test are examined. It is seen that the amount of deviations at the 5. welding point is found to be larger on the X axis. At the 3. and 4. welding points, the amount of deviations at the X axis is observed to be less. In the equilibrium test, there is a minimum deviation of -122.8 mm and a maximum of 93.26 mm on the X-axis. Moreover, a minimum deviation of -76.76 mm and a maximum of 77.03 mm on the Y-axis were observed. Consequently, it is seen in the Master thesis that if the conventional robot programming without vision based positioning is used the tests would fail in large part. The position changes of welding points in the are detected image-based robot positioning and the tests were successfully performed with the ABB IRB 140 robot.

REFERENCES

[1] Cheng, F. S. (2008). Calibration of robot reference frames for enhanced robot positioning accuracy. In *Robot Manipulators*. InTech.

[2] Gordić, Z., and Ongaro, C. (2016). Calibration of robot tool centre point using camera-based system. *Serbian Journal of Electrical Engineering*, *13*(1), 9-20.

[3] Borrmann, C., and Wollnack, J. (2015). Enhanced calibration of robot tool centre point using analytical algorithm. *Int J Mater Sci Eng*, *3*(1), 12-18.

[4] Bergström, G. (2011). Method for calibrating of off-line generated robot program.

[5] Wu, C. C., and Tang, G. R. (1998). Tolerance design for products with asymmetric quality losses. International Journal of Production Research, 36(9), 2529-2541.

[6] Balch, T., and Arkin, R. C. (1998). Behavior-based formation control for multirobot teams. IEEE transactions on robotics and automation, 14(6), 926-939.

[7] Hägele, M., Nilsson, K., Pires, J. N. (2008). Industrial robotics. In *Springer handbook of robotics* (pp. 963-986). Springer, Berlin, Heidelberg.

[8] Devol, J. G. C. (1961). *U.S. Patent No. 2,988,237*. Washington, DC: U.S. Patent and Trademark Office.

[9] Nof, S. Y. (Ed.). (1999). *Handbook of industrial robotics* (Vol. 1). John Wiley & Sons.

[10] IFR statiscal department (2014). *Industrial Robots 2014.* Executive Summary. International Federation of Robotics.

[11] Vistein, M. (2015). *Embedding Real-Time Critical Robotics Applications in an Object-Oriented Language* (Doctoral dissertation, University of Augsburg).

[12] RAPID Reference Manual. (2014). *ABB Group***.**

[13] KUKA System Software 8.3. Operating and Programming Instructions for System Integrators. (2014). *Version KSS 8.3 SI V3 en. KUKA Roboter GmbH*, 28 May 2010.

[14] VAL3 Reference Manual. (2010). *Staubli***,** 23 August 2010.

[15] Wells, G., and Torras, C. (2001). Assessing image features for vision-based robot positioning. *Journal of Intelligent and Robotic Systems*, 30(1), 95-118.

[16] Patoommakesorn, K., Vignat, F., Villeneuve, F. (2016). A new straight line matching technique by integration of vision-based image processing. *Procedia CIRP*, 41, 777-782.

[17] Ahmad, M. B., and Choi, T. S. (1999). Local threshold and boolean function based edge detection. *IEEE Transactions on Consumer Electronics*, *45*(3), 674-679.

[18] Wells, G., Venaille, C., Torras, C. (1996). Vision-based robot positioning using neural networks. Image and Vision Computing, 14(10), 715-732.

[19] Corke, P. I. (1993). Visual control of robot manipulators–a review. In Visual Servoing: Real-Time Control of Robot Manipulators Based on Visual Sensory Feedback, 1-31.

[20] Venaille, C., Wells, G., Torras, C. (1994). Application of neural networks to image-based control of robot arms. In *Intelligent Components and Instruments for Control Applications 1994*, 265-270.

[21] Masaki, I., Decker, S., Gupta, A., Horn, B. K. P., Lee, H. S., Martin, D. A., ... Wyatt, J. L. (1994, October). Cost-effective vision systems for intelligent vehicles. In *Intelligent Vehicles' 94 Symposium, Proceedings of the*, 39-43.

[22] Moon, S., and Virk, G. S. (2009). Survey on ISO standards for industrial and service robots. In *ICCAS-SICE,* 2009, 1878-1881.

[23] Vistein, M. (2015). Embedding Real-Time Critical Robotics Applications in an Object-Oriented Language (Doctoral dissertation, University of Augsburg).

[24] Sciavicco, L., & Siciliano, B. (2012). *Modelling and control of robot manipulators.* Springer Science & Business Media.

[25] Baran, Y., Rabenorosoa, K., Laurent, G. J., Rougeot, P., Andreff, N., Tamadazte, B. (2017, September). Preliminary results on OCT-based position control of a concentric tube robot. In *Intelligent Robots and Systems (IROS), 2017 IEEE/RSJ International Conference*, 3000-3005.

[26] Horn, B. (1986). *Robot vision*. MIT press.

[**27] Becedas, J., Payo, I., Feliu, V.** (2011). Two-flexible-fingers gripper force feedback control system for its application as end effector on a 6-DOF manipulator. *IEEE Transactions on Robotics*, *27*(3), 599-615.

[28] Kawasaki, H., Komatsu, T., Uchiyama, K. (2002). Dexterous anthropomorphic robot hand with distributed tactile sensor: Gifu hand II. *IEEE/ASME transactions on mechatronics*, *7*(3), 296-303.

[29] Ferrolho, A., and Crisóstomo, M. (2007). Intelligent control and integration software for flexible manufacturing cells. *IEEE Transactions on Industrial Informatics*, 3(1), 3-11.

[30] Carter, T. J. (2009). The Modeling of a Six Degree-of-freedom Industrial Robot for the Purpose of Efficient Path Planning.

[31] Vicente, D. B. (2007). *Modeling and Balancing of Spherical Pendulum Using a Parallel Kinematic Manipulator.* Department of Automatic Control, Lund University.

[32] Craig, J. J. (2005). *Introduction to robotics: mechanics and control* (Vol. 3, pp. 48-70). Upper Saddle River, NJ, USA:: Pearson/Prentice Hall.

[33] Hallenberg, J. (2007). Robot tool center point calibration using computer vision.

[34] Norberto Pires, J. (2005). Robot-by-voice: Experiments on commanding an industrial robot using the human voice. *Industrial Robot: An International Journal*, *32*(6), 505-511.

[35] Vijayan, A. T., and Ashok, S. (2017). Integrating visual guidance and feedback for an industrial robot. In *Control and Robotics Engineering (ICCRE), 2017 2nd International Conference on*, 18-22.

[36] Sujatha, K., Ponmagal, R. S., Godhavari, T. (2016). Automation of Solar System for Maximum Power Point Tracking using IoT. In *Proceedings of the International Conference on Informatics and Analytics.*

[37] Dubey, S. R., Dixit, P., Singh, N., Gupta, J. P. (2013). Infected fruit part detection using K-means clustering segmentation technique. *Ijimai*, *2*(2), 65-72.

[38] Christe, S. A., Vignesh, M., Kandaswamy, A. (2012). An efficient FPGA implementation of MRI image filtering and tumor characterization using Xilinx system generator.

[39] Bhargavi, K., and Jyothi, S. (2014). A survey on threshold based segmentation technique in image processing. *International Journal of Innovative Research and Development*, *3*(12).

[40] Jayaraman, S., and Esakkirajan, S. (2009). Digital image processing.

[41] Raju, P. D. R., and Neelima, G. (2012). Image segmentation by using histogram thresholding. *International Journal of Computer Science Engineering and Technology*, *2*(1), 776-779.

[42] Ravi, S., and Khan, A. M. (2013). Morphological Operators for Image Processing: Understanding and its Applications. In *NCVSComs-13 Conference Proceedings*, 17-19.

[43] Ravindran, G., Titus, T. J., Pravin, M., Pandiyan, P. (2017). Determination and Classification of Blood Types using Image Processing Techniques. *International Journal of Computer Applications*, *157*(1).

[44] Sato, K. (2003). *U.S. Patent No. 6,515,704*. Washington, DC: U.S. Patent and Trademark Office.

[45] Jiang, M., Shi, J., Ma, H., Li, Y. (2017). A vision and neural network based air-ground coordinated control system. In *Unmanned Systems (ICUS), 2017 IEEE International Conference on* (pp. 488-493). IEEE.

[46] Lv, J., and Li, Z. The Research of Machine Vision Motion Control System based on the Labview.

[47] Goldberg, M., Truman, J. C., Kniffin, A. B. (2006). *U.S. Patent No. 7,055,262*. Washington, DC: U.S. Patent and Trademark Office.

[48] Aktaş, M., Ceylan, İ., Yilmaz, S. (2009). Determination of drying characteristics of apples in a heat pump and solar dryer. *Desalination*, *239*(1-3), 266-275.

[49] Rahman, M. S., Perera, C. O., Thebaud, C. (1997). Desorption isotherm and heat pump drying kinetics of peas. *Food Research International*, *30*(7), 485-491.

[50] Teeboonma, U., Tiansuwan, J., Soponronnarit, S. (2003). Optimization of heat pump fruit dryers. *Journal of Food Engineering*, *59*(4), 369-377.

[51] Rinehart, C. M. (2004). *U.S. Patent No. 6,772,598*. Washington, DC: U.S. Patent and Trademark Office.

[52] Malis, E. (2002). Survey of vision-based robot control. *ENSIETA European Naval Ship Design Short Course, Brest, France*, *41*, 46.

[53] Hager, G. D., Chang, W. C., Morse, A. S. (1994). Robot feedback control based on stereo vision: Towards calibration-free hand-eye coordination. In *Robotics and Automation, 1994. Proceedings., 1994 IEEE International Conference on*, 2850-2856.

[54] Feddema, J. T., Lee, C. G., Mitchell, O. R. (1991). Weighted selection of image features for resolved rate visual feedback control. *IEEE Transactions on Robotics and Automation*, *7*(1), 31-47.

[55] Kelly, R. (1996). Robust asymptotically stable visual servoing of planar robots. *IEEE Transactions on Robotics and Automation*, *12*(5), 759-766.

[56] Nikolskyy, A. I., Krasilenko, V. G., Bilynsky, Y. Y., Starovier, A. (2017). Using LabView for real-time monitoring and tracking of multiple biological objects. In *Health Monitoring of Structural and Biological Systems 2017*.

CURRICULUM VITAE

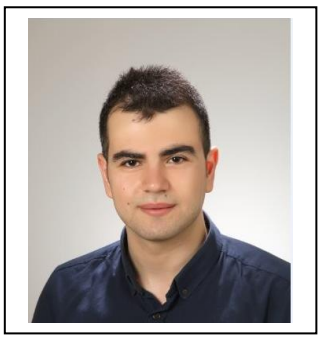

Name Surname: Akın İlker Savran

Place and Date of Birth: Bakırköy/İstanbul, 09.09.1989

E-Mail: savran@itu.edu.tr

EDUCATION :

- **B.Sc.** **:** 2015, Istanbul Techincal University, Faculty of Electrical and Electronics Engineering , Control and Automation Engineering Department

PROFESSIONAL EXPERIENCE AND REWARDS:

- 2013-2016 Researcher at ABB Process Control and Automation Laboratory
- 2014-2015 Application Consultant at LA Software Group
- 2015-2016 Researcher at Getron Software
- 2016-… Automation Engineer of Production Engineering at Arçelik
- 2015 Best Undergraduate Thesis Award at Elektrik Tesisat Mühendisleri Dernegi (ETMD)

OTHER PUBLICATIONS, PRESENTATIONS AND PATENTS:

- Yesil, E., **Savran, A. I.,** and Guzay, C. (2014). Load frequency controller design using new Big Bang-Big Crunch 2 algorithm. In *Innovations in Intelligent Systems and Applications (INISTA) Proceedings, 2014 IEEE International Symposium on*(pp. 7-13). IEEE.
- **Savran, A. I.,** Musaoglu, E., Yuce, M. F., and Yesil, E. (2014). RouteArt: A new framework for vehicle routing problem with pickup and delivery using heuristic bubble algorithm. In *Computational Intelligence and Informatics (CINTI), 2014 IEEE 15th International Symposium on* (pp. 91-96). IEEE.

- **Savran, A. I.,** Musaoglu, E., Yildiz, C., Yuce, M. F., and Yesil, E. (2015). Extended heuristic bubble algorithm for the pickup and delivery problem with time windows. In *Applied Machine Intelligence and Informatics (SAMI), 2015 IEEE 13th International Symposium on* (pp. 145-150). IEEE.
- **Savran, A. I.,** Musaoglu, E., Yildiz, C., and Yuce, M. F. (2015). An efficient solution to Location-Routing Problems via a two-phase heuristic bubble approach. In *Advanced Logistics and Transport (ICALT), 2015 4th International Conference on* (pp. 169-174). IEEE.
- **Savran, A. I.,** Beke, A., Kumbasar, T., and Yesil, E. (2015). An IMC based fuzzy self-tuning mechanism for fuzzy PID controllers. In *Innovations in Intelligent SysTems and Applications (INISTA), 2015 International Symposium on* (pp. 1-7). IEEE.
- **Savran A. I.,** Beke A., Kumbasar T., and Yesil, E., (2015). Design of PID Controller with IMC Based Gain-Scheduling Mechanism for Extruder Processes. Turkish National Meeting on Automatic Control, *Otomatik Kontrol Ulusal Toplantısı (TOK 2015)*, Denizli, Türkiye.
- Dodurka, M. F., Sakalli, A., Beke, A., **Savran, A. I.,** Sahin, A., Kumbasar, T., Yesil, E., and Hagras, H., (2015). Vehicle Platoon Control: Consensus Based Approach," Turkish National Meeting on Automatic Control, *Otomatik Kontrol Ulusal Toplantısı (TOK 2015)*, Denizli, Türkiye.